

How accurately can the climate sensitivity to CO₂ be estimated from historical climate change?

Article

Accepted Version

Gregory, J. M. ORCID: <https://orcid.org/0000-0003-1296-8644>,
Andrews, T., Ceppi, P., Mauritsen, T. and Webb, M. J. (2020)
How accurately can the climate sensitivity to CO₂ be estimated
from historical climate change? *Climate Dynamics*, 54 (1-2).
pp. 129-157. ISSN 0930-7575 doi:
<https://doi.org/10.1007/s00382-019-04991-y> Available at
<https://centaur.reading.ac.uk/86308/>

It is advisable to refer to the publisher's version if you intend to cite from the work. See [Guidance on citing](#).

To link to this article DOI: <http://dx.doi.org/10.1007/s00382-019-04991-y>

Publisher: Springer

All outputs in CentAUR are protected by Intellectual Property Rights law, including copyright law. Copyright and IPR is retained by the creators or other copyright holders. Terms and conditions for use of this material are defined in the [End User Agreement](#).

www.reading.ac.uk/centaur

CentAUR

Central Archive at the University of Reading

Reading's research outputs online

1 **How accurately can the climate sensitivity to CO₂**
2 **be estimated from historical climate change?**

3 **J. M. Gregory***, T. Andrews, P. Ceppi,
4 **T. Mauritsen, M. J. Webb**

5
6 17 September 2019

7 **Abstract** The equilibrium climate sensitivity (ECS, in K) to CO₂ doubling is a large
8 source of uncertainty in projections of future anthropogenic climate change. Esti-
9 mates of ECS made from non-equilibrium states or in response to radiative forcings
10 other than $2 \times \text{CO}_2$ are called “effective climate sensitivity” (EffCS, in K). Taking a
11 “perfect-model” approach, using coupled atmosphere–ocean general circulation model
12 (AOGCM) experiments, we evaluate the accuracy with which CO₂ EffCS can be esti-
13 mated from climate change in the “historical” period (since about 1860). We find that
14 (1) for statistical reasons, unforced variability makes the estimate of historical EffCS
15 both uncertain and biased; it is overestimated by about 10% if the energy balance is
16 applied to the entire historical period, 20% for 30-year periods, and larger factors for
17 interannual variability, (2) systematic uncertainty in historical radiative forcing trans-
18 lates into an uncertainty of $\pm 30\text{--}45\%$ (standard deviation) in historical EffCS, (3) the
19 response to the changing relative importance of the forcing agents, principally CO₂ and
20 volcanic aerosol, causes historical EffCS to vary over multidecadal timescales by a factor
21 of two. In recent decades it reached its maximum in the AOGCM historical experiment
22 (similar to the multimodel-mean CO₂ EffCS of 3.6 K from idealised experiments), but
23 its minimum in the real world (1.6 K for an observational estimate for 1985–2011,
24 similar to the multimodel-mean value for volcanic forcing). The real-world variations
25 mean that historical EffCS underestimates CO₂ EffCS by 30% when considering the
26 entire historical period. The difference for recent decades implies that either unforced
27 variability or the response to volcanic forcing causes a much stronger regional pattern
28 of sea surface temperature change in the real world than in AOGCMs. We speculate

* j.m.gregory@reading.ac.uk, ORCID 0000-0003-1296-8644

J. M. Gregory
National Centre for Atmospheric Science, University of Reading, UK
and Met Office Hadley Centre, Exeter, UK

T. Andrews and M. J. Webb
Met Office Hadley Centre, Exeter, UK

P. Ceppi
Grantham Institute, Imperial College London, UK

T. Mauritsen
Department of Meteorology, Stockholm University, Sweden

that this could be explained by a deficiency in simulated coupled atmosphere–ocean feedbacks which reinforce the pattern (resembling the Interdecadal Pacific Oscillation in some respects) that causes the low EffCS. We conclude that energy-balance estimates of CO₂ EffCS are most accurate from periods unaffected by volcanic forcing. Atmosphere GCMs provided with observed sea surface temperature for the 1920s to the 1950s, which was such a period, give a range of about 2.0–4.5 K, agreeing with idealised CO₂ AOGCM experiments; the consistency is a reason for confidence in this range as an estimate of CO₂ EffCS. Unless another explosive volcanic eruption occurs, the first 30 years of the present century may give a more accurate energy-balance historical estimate of this quantity.

Keywords climate sensitivity; climate feedback; volcanic forcing

1 Introduction

The equilibrium climate sensitivity (ECS), defined as the steady-state global-mean surface air temperature change due to a doubling of the atmospheric carbon dioxide concentration, has been used for decades as a benchmark for the magnitude of climate change predicted by general circulation models (GCMs) in response to CO₂ increase. Although an equilibrium climate is not expected in the future, ECS is relevant to future climate change because it correlates with global warming under realistic time-dependent scenarios for the future, which are dominated by CO₂ increase (Gregory et al 2015; Knutti et al 2017; Grose et al 2018). Over the past 25 years, GCMs have considerably improved in their simulation of present climate and historical climate change (Reichler and Kim 2008; Flato et al 2013, where by “historical” we mean since the 19th century), but their ECS has had a persistently wide spread. The range of ECS simulated by GCMs was 1.9–5.2 K (Mitchell et al 1990) when assessed in the first Assessment Report of the Intergovernmental Panel on Climate Change, and 2.1–4.7 K in the most recent (the Fifth Assessment Report, AR5, Flato et al 2013).

This uncertainty has stimulated efforts to evaluate the ECS from observed historical climate change. One common approach is to apply the global-mean energy balance of the climate system

$$N = F - R = F - \alpha T, \quad (1)$$

where F is the effective radiative forcing (ERF, Myhre et al 2013, calculated from observed or estimated forcing agents), N is the global-mean net downward radiative flux at the top of the atmosphere (TOA) *i.e.* the heat flux into the climate system, T is the global-mean surface temperature change with respect to an unperturbed equilibrium in which $N = F = 0$, and $R = F - N = \alpha T$ is the radiative response of the system to change in T . Note that F is positive downwards, while R is positive upwards.

Our α in Equation (1) is the *positive-stable* climate feedback parameter ($\text{W m}^{-2} \text{K}^{-1}$), with $\alpha > 0$ so that $R = \alpha T$ resists F . This sign convention is convenient for our purposes. Some papers on this subject use a *negative-stable* climate feedback parameter λ , numerically the same as ours but with $+\lambda T$ instead of $-\alpha T$ in Equation (1). The advantage of that convention is that those processes which are positive feedbacks in a physical sense *e.g.* water vapour feedback, tending to amplify T , make positive contributions to the net λ , which is negative. The reciprocal of $\alpha (= -\lambda)$ is the climate sensitivity parameter $S = 1/\alpha$ ($\text{K W}^{-1} \text{m}^2$); the larger α , the smaller S . This quantity is always given a positive sign, regardless of the sign convention for α .

The energy balance (Equation 1) implies that $ECS = F_{2\times}/\alpha$, where $F_{2\times}$ is the ERF of $2\times CO_2$, since $N = 0$ in the perturbed equilibrium. Thus a larger α implies a smaller ECS. When α is estimated from climate change which has not reached equilibrium (whether historical, future or under idealised scenarios), $F_{2\times}/\alpha = SF_{2\times}$ is called the “effective climate sensitivity” (EffCS), which equals the ECS only if α is a constant, as was formerly assumed (*e.g.* by Gregory et al 2002, among many others). The usual method to estimate α in CMIP5 is from Equation (1), by regression of N against T for the *abrupt4xCO2* experiment, in which CO_2 is instantaneously quadrupled at $t = 0$ with respect to the control state (Gregory et al 2004). Recent work shows that historical climate change tends to give a larger median estimate of α , and hence a smaller EffCS, than GCMs do under idealised high- CO_2 scenarios, such as *abrupt4xCO2*, which have ERF of the magnitude typically projected for the 21st century (Forster 2016).

Since the unperturbed equilibrium is not a known historical state, in practice Equation (1) is applied to the differences (denoted by Δ , in N , F and T) between two historical states (Gregory et al 2002; Otto et al 2013)

$$\alpha = \frac{\Delta R}{\Delta T} = \frac{\Delta F - \Delta N}{\Delta T} \quad (2)$$

or by regression in the differential form

$$\alpha = \frac{dR}{dT} = \frac{d}{dT}(F - N). \quad (3)$$

Both Equation (2) and Equation (3) eliminate the unknown equilibrium state. If data is available throughout the period of interest, regression (Equation 3) is a more efficient estimator of the slope than differences (Barnes and Barnes 2015). Either way, this is a modified version of the method of Gregory et al (2004), following Forster and Gregory (2006) and Tett et al (2007), for the situation where F is time-dependent. Many studies have estimated α from real-world historical F , N and T using Equation (1), (2) or (3) in various ways (examples are cited in the review by Knutti et al 2017).

ERF F is not an observable quantity, and has to be calculated using models of radiative transfer, calibrated formulae (*e.g.* supplementary material of Myhre et al 2013) and atmosphere GCM (AGCM) experiments (Section 3.1; Hansen et al 2005). Therefore historical F is a source of systematic uncertainty in estimating α , especially on account of anthropogenic tropospheric aerosol forcing (Gregory et al 2002; Myhre et al 2013; Forster 2016; Skeie et al 2018).

Historical N is a source of statistical uncertainty in estimating α , due to the combination of two circumstances. First, internally generated *i.e.* unforced variations in the climate system add statistical “noise” to the externally forced signal in N . Second, the comparative shortness of the observational record of N limits the possibility of reducing the imprecision due to the noise. N can be evaluated reasonably precisely from satellite measurements of the global TOA Earth radiation budget, especially by the Earth Radiation Budget Experiment (ERBE) during 1985–1988 and by the Clouds and Earth’s Radiant Energy System (CERES) since 2000, and of global ocean temperature measurements by Argo floats since 2005 (Allan et al 2014; Roemmich et al 2015; Palmer 2017). N can be estimated less precisely from the sparser ocean temperature measurements made by ships back to the 1960s, but hardly at all for earlier decades (Abraham et al 2013).

An alternative method for estimating α (Section 6.1) has recently been developed, using an AGCM experiment called *amip-piForcing*, in which observed sea surface temperature (SST) is a boundary condition, to which simulated N responds (Gregory and

Table 1 Notation for the climate feedback parameter.

In this paper $\alpha > 0$ is the positive-stable climate feedback parameter ($\text{W m}^{-2} \text{K}^{-1}$), evaluated as the slope from regression of the global-mean annual-mean radiative response R against surface air temperature change T , from real-world estimates or from ensembles of historical simulations with AOGCMs and AGCMs. Various choices for the regression are denoted as shown in the table, second column for the entire historical period (labelled “All”, time-independent and marked with an overbar), third for 30-year periods (labelled “30”, time-dependent and marked with a tilde) where $\tilde{\alpha}(t)$ applies to the 30 years centred on time t . Lower-case subscripts denote ensemble means of integrations from individual models, upper-case denote multimodel means.

Real world or a single integration	All	30
Mean of slopes of R against T from individual integrations of a single model	$\bar{\alpha}_i$	$\tilde{\alpha}_i$
Slope of ensemble-mean R against T of a single model	$\bar{\alpha}_e$	$\tilde{\alpha}_e$
Multimodel mean of slopes of ensemble-mean R against T from individual models	—	$\tilde{\alpha}_I$
Slope of multimodel-mean ensemble-mean R against T	$\bar{\alpha}_E$	$\tilde{\alpha}_E$

117 Andrews 2016; Zhou et al 2016; Andrews et al 2018). This method does not involve
 118 knowing real historical F and N , and thus avoids the uncertainties associated with
 119 these quantities. The *amip-piForcing* experiment gives a larger α (smaller EffCS) for
 120 historical climate change than experiments using the same AGCMs, incorporated in
 121 coupled atmosphere–ocean GCMs (AOGCMs), to simulate the response to $4 \times \text{CO}_2$.
 122 Moreover, *amip-piForcing* shows substantial decadal historical variation in α .

123 For any transient climate state, the EffCS and α quantify the relationship between
 124 changes in global-mean R and global-mean T , determined by the response to SST of
 125 surface and atmospheric processes which affect TOA radiation. The AOGCM, AGCM
 126 and energy-budget analyses provide evidence that α is not constant in various ways.
 127 We can distinguish two kinds of reason for the inconstancy of α . First, α might depend
 128 on the magnitude of global-mean T or F , which could be formalised by making Equa-
 129 tion (1) non-linear in these quantities (Meraner et al 2013; Good et al 2012; Gregory
 130 et al 2015; Bloch-Johnson et al 2015). Second, R and α may vary because of changes
 131 in the pattern of SST, *i.e.* “pattern effects” (Stevens et al 2016; Gregory and Andrews
 132 2016; Ceppi and Gregory in press). Such effects cannot be predicted by Equation (1),
 133 because it deals only with global means, and it becomes nonsensical in limiting cases.
 134 For instance, if changing SSTs alter R but not T , α is infinite and EffCS is zero.

135 The inconstancy of α raises the question which is the title of this paper. To address
 136 the question, we analyse AOGCM simulations of the historical period. The analysis
 137 has two aspects. First, we evaluate how accurately we would be able to estimate the
 138 EffCS for CO_2 forcing from the historical record if the real world truly behaved like
 139 an AOGCM *i.e.* a “perfect-model” test. The AOGCMs enable this investigation be-
 140 cause they provide complete datasets for many alternative realisations of the historical
 141 period, whereas the historical period has occurred only once in the real world and
 142 the observational dataset of it is incomplete. Second, we investigate the causes of the
 143 time-variation of α in the historical period. We make use of AOGCM experiments that
 144 simulate change due to unforced variability alone and to subsets of historical forcings,
 145 whereas we cannot control these influences in the real world.

146 In Section 2 we give details of the AOGCM experiments, and in Section 3 we
 147 derive estimates of F for the AOGCMs. In Section 4 we show that, if the AOGCMs

Table 2 List of models whose results are analysed in this work, showing the number of members in their ensembles. The *amip-piForcing* experiment uses only the AGCM component of the AOGCM identified.

AOGCM	<i>historical</i>	<i>historicalGHG</i>	<i>historicalNat</i>	<i>amip-piForcing</i>
<hr/> CMIP5 models <hr/>				
ACCESS1-0	2			
ACCESS1-3	3	2		
CNRM-CM5	10	5	6	
CSIRO-Mk3-6-0	10	5	5	
CanESM2	5	5	5	
GFDL-CM3	5	3	3	6
GFDL-ESM2M	1	1	1	5
GFDL-ESM2G	3			
HadGEM2-ES	5	4	3	4
IPSL-CM5A-LR	6	6	3	
MIROC-ESM	3	3	3	
MIROC5	5			
MPI-ESM-LR	3			
MPI-ESM-MR	3			
MRI-CGCM3	5	1	1	
NorESM1-M	3	1	1	
<hr/> Other models <hr/>				
HadCM3				4
MPI-ESM1.1	100			5

148 are realistic, dR/dT evaluated from historical climate change by Equation (3) may be
 149 an imprecise and biased estimate of the historical α , owing to the statistical effects of
 150 unforced variability. In Section 5 we show that α varies during the historical period
 151 in response to the changing nature of the forcing, which is not due to CO_2 alone.
 152 The AOGCMs indicate that the most recent decades should have α closest to its
 153 CO_2 value, but in Section 6 we present evidence that the historical time-variation
 154 of α in the AOGCMs may be unrealistic in that regard, by comparison with AGCM
 155 *amip-piForcing* experiments. We conclude in Section 7 by discussing the answer to
 156 the question posed by the paper, in view of the statistical and systematic errors in
 157 estimating the CO_2 α from the historical α .

158 Throughout the paper, uncertainties written with \pm in the text and shown by
 159 coloured shading in the diagrams are one standard deviation or one standard error (as
 160 appropriate). Our notation for different methods of estimating α , discussed throughout
 161 the paper, is summarised in Table 1.

162 2 AOGCM historical experiments

163 We analyse results from the *historical*, *historicalNat* and *historicalGHG* experiments
 164 from 16 AOGCMs of the Coupled Model Intercomparison Project Phase 5 (CMIP5,
 165 Table 2). Climate change is calculated with respect to the *piControl* experiment, which
 166 has constant pre-industrial forcing agents. The *historical*, *historicalGHG* and *histori-*
 167 *calNat* experiments begin in the latter part of the 19th century from *piControl* states,
 168 and run to 2005 with time-dependent historical changes in forcing agents. The *histor-*
 169 *ical* experiment includes all changes in atmospheric composition, anthropogenic and
 170 volcanic aerosols, solar irradiance and land-use; *historicalGHG* includes changes only

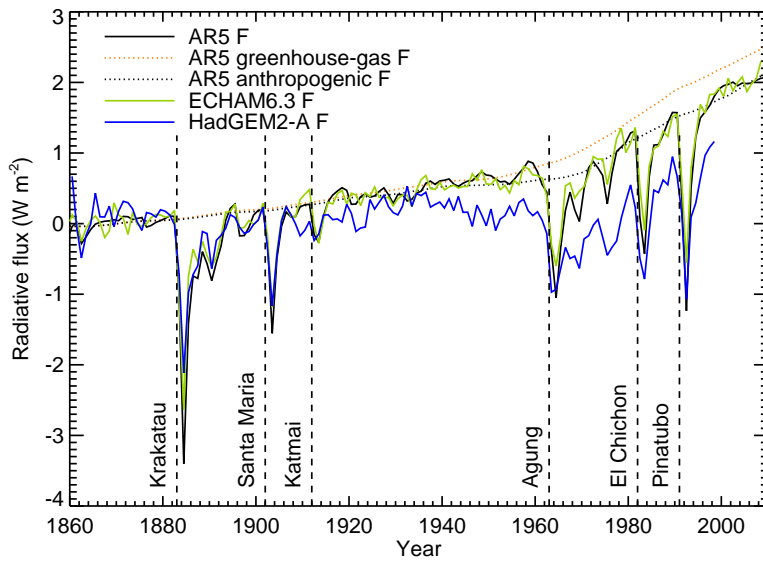


Fig. 1 Comparison of the AR5 estimate of annual-mean *historical* ERF $F(t)$, relative to the 1860–1879 time-mean (a period without large volcanic eruptions, approximating pre-industrial), with diagnoses of $F(t)$ from *piClim-histall* and *piClim-control* experiments using the ECHAM6.3 and HadGEM2-A AGCMs. The vertical dashed lines indicate the years of major volcanic eruptions.

171 in greenhouse gas concentrations, *historicalNat* only in the natural forcing agents of
 172 volcanic aerosol and solar irradiance.

173 Unforced interannual variability in T (pooled standard deviation of 0.11 K in the
 174 AOGCM *piControl* experiments) is not negligible compared with the change in T
 175 during the historical period (about 0.8 K, depending on definition, Hartmann et al
 176 2013). Therefore, in order to clarify the forced signal, historical experiments with most
 177 AOGCMs have been run as ensembles of various sizes, with each integration in the
 178 ensemble beginning from a different state in the *piControl* experiment. Provided the
 179 states are sufficiently separated, the unforced variability in the ensemble members is
 180 not correlated, and its temporal standard deviation is a factor $1/\sqrt{N}$ smaller in the
 181 ensemble mean of N integrations than in each individually.

182 The CMIP5 historical ensembles have no more than 10 members and fewer in
 183 most cases (Table 2). We also use a much larger *historical* ensemble of 100 members
 184 carried out with the MPI-ESM1.1 AOGCM, which is an updated version of the CMIP5
 185 AOGCM of Giorgetta et al (2013). We assume that variations in global climate in the
 186 mean of this ensemble are mostly the response to forcing, since unforced variability is
 187 reduced by a factor of 10. This makes it very useful in a perfect-model approach, since
 188 we can obtain an accurate estimate of its true α , provided we know F , which is the
 189 subject of the next section.

190 3 Historical radiative forcing

191 To apply the global-mean energy balance to observed climate change, we need to know
 192 historical ERF. Myhre et al (2013, AR5) estimated $F(t)$ from historical emissions and
 193 atmospheric composition, radiative transfer calculations, and a variety of models. The
 194 net forcing goes up as greenhouse gas concentrations increase, partly compensated by
 195 negative ERF from anthropogenic aerosols (our Figure 1, their Figure 8.18). There is a
 196 large negative spike for a small number of years following each major volcanic eruption,
 197 due to reflection of sunlight by aerosol formed from sulphur dioxide injected into the
 198 stratosphere. A wide systematic uncertainty range of 1.1–3.3 W m^{-2} is given for the
 199 net anthropogenic ERF at 2011 relative to 1750.

200 In the following sections we diagnose α from CMIP5 *historical* experiments using
 201 Equation (1). For that purpose we need to know F in the AOGCMs, which may be
 202 substantially different from the real world F , on account of various model errors. The
 203 object of this section is to estimate the model F .

204 3.1 Diagnosis using AGCMs

205 The *historical* $F(t)$ can be diagnosed for an AOGCM by running a pair of experiments
 206 with the AGCM alone, having prescribed unchanging climatological pre-industrial sea
 207 surface temperature and sea ice concentration. One of the experiments, called *piClim-*
 208 *histall*, has time-dependent atmospheric composition and land use for the historical
 209 period, while the other is a control, called *piClim-control*, with constant pre-industrial
 210 forcings (Hansen et al 2005; Held et al 2010; Andrews 2014; Pincus et al 2016).

211 If we assume, despite the forcing, that the surface boundary conditions enforce the
 212 same surface temperature in the two experiments, $T = 0 \Rightarrow F = N$ for the difference in
 213 energy balance (Equation 1) between them. That is, the *historical* ERF equals the net
 214 input N of energy to the climate system due to the forcing agents. Surface temperature
 215 is free to change over land, for practical reasons (*e.g.* Kamae et al 2019), giving $T \simeq 10\%$
 216 of the equilibrium T (Andrews et al 2012, red crosses in their Figure 1). This effect
 217 has not been quantified for CMIP5 *historical* simulations, but it will be possible to
 218 quantify it in CMIP6 using the experiments *piClim-histall* and *piClim-control*.

219 We have run the experiments with the ECHAM6.3 and HadGEM2-A AGCMs to
 220 obtain $F(t)$ for MPI-ESM1.1 and HadGEM2-ES AOGCMs, which incorporate these
 221 AGCMs respectively. The ECHAM6.3 (MPI-ESM1.1) $F(t)$ is very close to the AR5
 222 estimate, whereas the HadGEM2 F increases considerably less (Figure 1), in part due
 223 to strong negative land-use forcing (Andrews et al 2017). The difference between these
 224 two models illustrates the possibly large but unknown spread in CMIP5 F .

225 3.2 Forcing due to tropospheric and volcanic aerosol

226 To examine the consistency between our set of AOGCMs and the AR5 regarding forc-
 227 ing, we estimate the *historical* annual-mean $T(t)$ expected in response to the AR5 $F(t)$
 228 with the “step model”, which uses $T(t)$ in response to a step-change in CO_2 in each
 229 AOGCM as a kernel to be convolved with the forcing timeseries (more detail given in
 230 Appendix A). The step-model mean shows more warming during the historical period
 231 than the AOGCM mean (Figure 2a). We suggest that this is because the AR5 F is

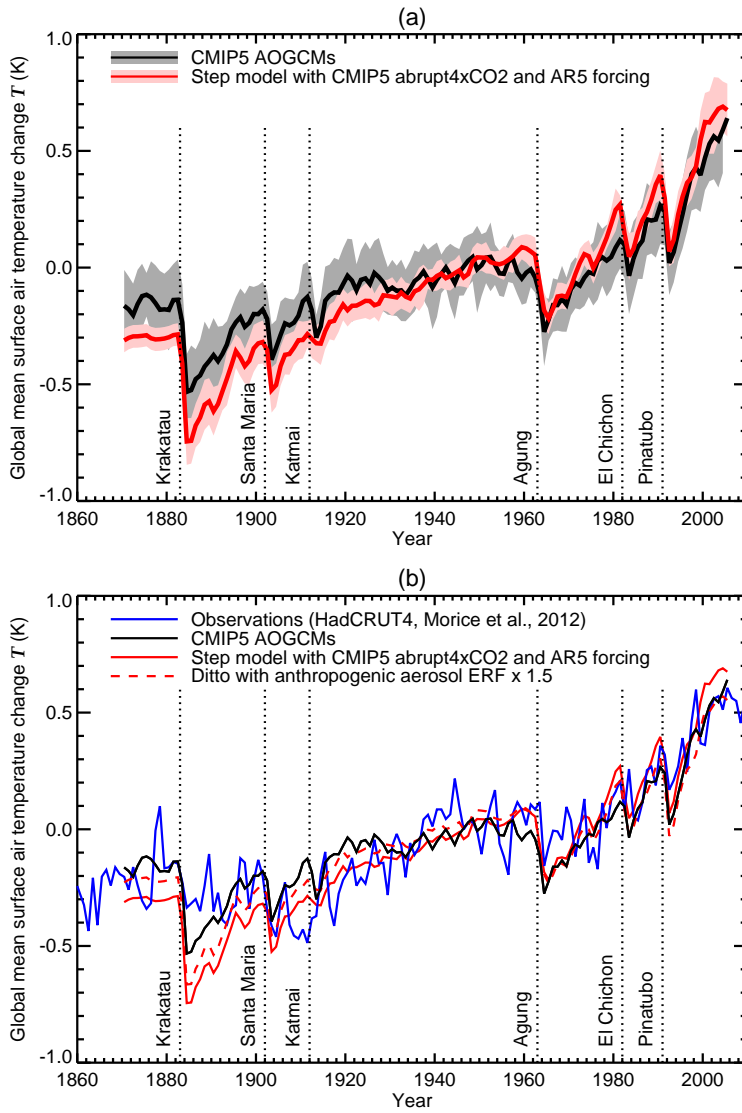


Fig. 2 Timeseries of historical global-mean annual-mean surface air temperature, relative to the time-mean of 1900–2005, from observations, from CMIP5 AOGCMs (using the ensemble mean for each AOGCM) and from the step-model emulation of CMIP5 using the AR5’ ERF timeseries with scaling factors (described in the text) applied to volcanic and anthropogenic aerosol ERF. The solid lines show the multimodel mean for the AOGCMs and the emulation of AOGCMs. In (a) the envelopes show the ensemble standard deviation, and (b) compares the multimodel means with the observational estimate.

larger than the AOGCM mean F , due to the negative anthropogenic aerosol forcing being stronger in AOGCMs than in reality, consistent with the expert judgement of Myhre et al (2013). Alternatively, EffCS may be larger for anthropogenic aerosol forcing than it is for CO_2 (*i.e.* efficacy greater than unity, defined at the start of Section 5; Hansen et al 2005; Shindell 2014; Marvel et al 2016; but *cf.* Paynter and Frölicher 2015). The step model implicitly assumes the same EffCS for all forcing agents.

The multimodel standard deviation of the step-model timeseries is 0.08 K (the pink envelope in Figure 2a, pooled over years), which must be due mostly to the AOGCM spread in climate feedback, because the step model uses the same AR5 F for all AOGCMs. The multimodel standard deviation of the AOGCM *historical* timeseries is 0.14 K (the grey envelope, pooled over years). If the standard deviation of unforced interannual variability in T in every AOGCM were 0.11 K, which is the pooled estimate from *piControl*, and if the 64 historical integrations (Table 2) were equally weighted (both of these are fair approximations), unforced variability would make a negligible contribution of $0.11/\sqrt{64} = 0.013$ K to the AOGCM *historical* multimodel standard deviation. Therefore we suggest that the multimodel standard deviation is larger for the AOGCMs than the step model because of the AOGCM spread in F . Since different choices have been made for numerous aspects of the formulation of AOGCMs, the actual ERF in a given CMIP5 *historical* run will not necessarily be the same as the AR5 median estimate for the real world.

To estimate the uncertainty in F from AOGCMs, we take $N \simeq F/3$ for the multimodel mean (Gregory and Forster 2008), whereby Equation (2) becomes $\alpha = (F - N)/T \simeq \frac{2}{3}F/T \Rightarrow T \simeq \frac{2}{3}F/\alpha$. Therefore the fractional uncertainty in T will be the sum in quadrature of the fractional uncertainties in α and historical F , which we assume to be uncorrelated (Forster et al 2013). For the time-mean of 1986–2005 (the reference period of the AR5 for projections) relative to the time-mean of 1860–1879 (our reference period for ERF in Figure 1), T has a standard deviation in the step model of about $\pm 15\%$. This uncertainty is attributable to α . It is negligible compared with the standard deviation in the AOGCMs in T of $\pm 45\%$, which must therefore be nearly entirely attributable to the AOGCM uncertainty in F . By comparison, if the AR5 likely range for F of 1.13–3.33 $\text{W m}^{-2} \text{K}^{-1}$ at 2011 relative to 1750 (Myhre et al 2013) is assumed to represent the 5–95% range of a normal distribution, its standard deviation is $\pm 30\%$.

We have evaluated the root-mean-square (RMS) difference in $T(t)$ for 1900 onwards between the step-model mean and the AOGCM mean as a function of a time-independent scaling factor applied to the AR5 timeseries of anthropogenic aerosol ERF. The smallest RMS difference, meaning the closest mean match of the step models to the AOGCMs (dashed red line in Figure 2b), is obtained by making the anthropogenic aerosol ERF 50% stronger (more negative) than the AR5 estimate. Consistent with this finding, the estimate by Zelinka et al (2014) of the anthropogenic aerosol ERF at 2000 relative to 1860 in a set of AR5 AGCMs is 1.6 ± 0.4 times larger than the AR5 median estimate.

It may also be noted that the negative spikes of F in volcano years are not as deep in the AGCMs as in the AR5 estimate (Figure 1). Linear regression of AGCM F against AR5 F for the years with strong volcanic forcing gives 0.78 for ECHAM6.3 and 0.58 for HadGEM2. This is qualitatively consistent with earlier findings that volcanic forcing is about 80% of the AR5 estimate in the mean of CMIP5 AOGCMs (Larson and Portmann 2016), and about 70% in the HadCM3 AOGCM (Gregory et al 2016),

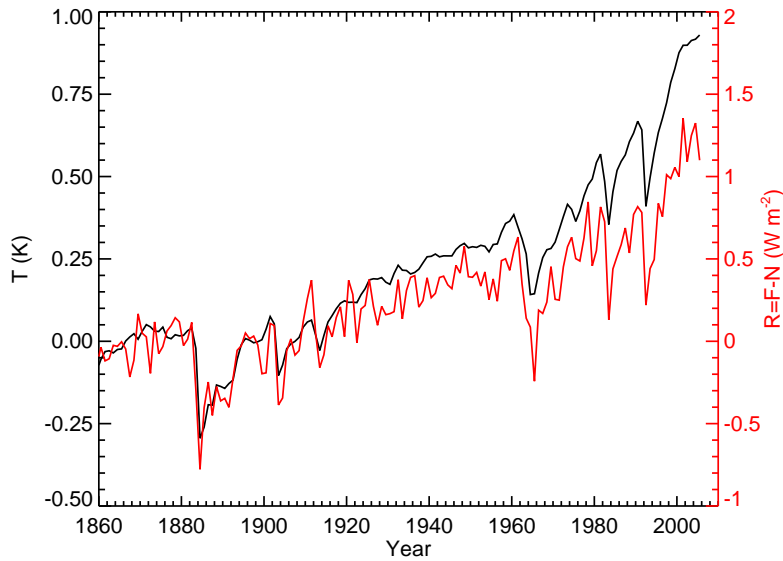


Fig. 3 Timeseries of ensemble-mean annual-mean global-mean surface air temperature T and radiative response $R = F - N$, both with respect to the unperturbed climate state, in the MPI-ESM1.1 *historical* experiment.

280 which the latter authors attributed to rapid cloud adjustments not included in the AR5
 281 estimate.

282 3.3 Estimate of CMIP5 historical forcing

283 To estimate the historical $F(t)$ in CMIP5 models, in view of the findings of this section,
 284 we multiply the AR5 volcanic F by 0.8 and the AR5 anthropogenic aerosol F by 1.5.
 285 Henceforth by “AR5’ forcing” we mean the AR5 F with these modifications. The AR5’
 286 F is *not* a revised estimate for the real world. We note that there there is a model spread
 287 of $\pm 45\%$, but we do not have estimates for individual CMIP5 models. In CMIP6, the
 288 historical F for each model will be diagnosed by the AGCM experiments of Section 3.1,
 289 which are included in the Radiative Forcing Model Intercomparison Project (RFMIP,
 290 Pincus et al 2016).

291 4 Using regression to estimate historical climate feedback

292 During the historical period, the net forcing grows, T rises, and the heat loss R to space
 293 increases. The 100-member MPI-ESM1.1 *historical* ensemble is useful to illustrate this
 294 behaviour because it is so large that the noise is fairly small in the ensemble mean, and
 295 because we have a diagnosis of F for this model (Section 3.1), enabling an accurate
 296 estimate of $R = F - N$. We see that the decadal trends of $R = F - N$ and T usually
 297 have the same sign, both usually being positive, and their interannual variability shows
 298 some similarity as well, especially regarding the negative excursions caused by volcanic
 299 forcing (Figure 3). Their agreement on these features means that the ensemble-mean

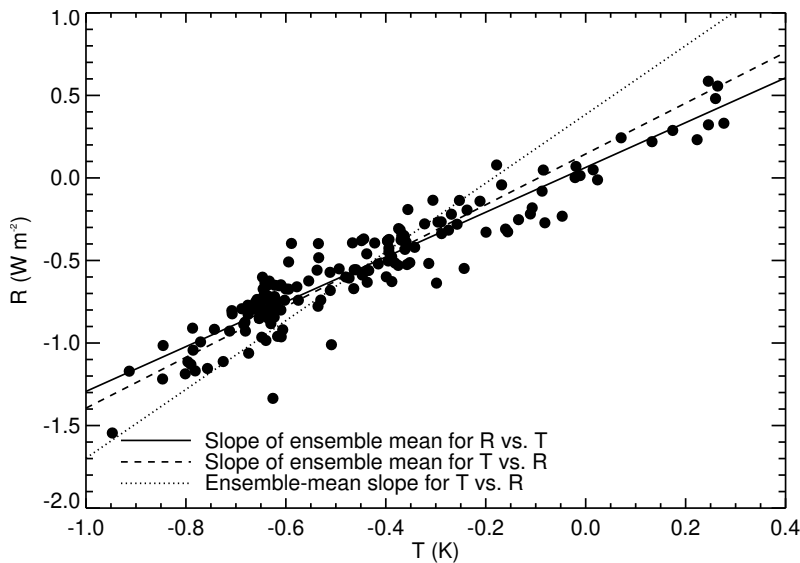


Fig. 4 Regression of annual-mean $R = N - F$ against T and vice-versa in the MPI-ESM1.1 *historical* experiment. The data points are annual-mean ensemble-mean values, with respect to the time-mean of the AMIP period 1979–2008, and the lines show regression slopes calculated as indicated.

300 annual-mean R and T are positively correlated (with coefficient of 0.94, Figure 4). This
 301 is consistent with the assumption $R = \alpha T$ of the energy balance (Equation 1), which
 302 motivates the estimation of α from the covariation of R and T .

303 In this section, we summarise some statistical issues that affect the accuracy of
 304 the estimate. Its findings are important to the interpretation of historical data, but
 305 its subject is a digression from the physical investigation. Therefore we have put the
 306 detailed discussion and mathematical demonstrations in appendices.

307 Following many other authors, we obtain α according to Equation (3) as the slope
 308 from linear regression of R against T . Unforced variability affects N and hence R ,
 309 making α statistically uncertain. From the MPI-ESM1.1 *historical* ensemble, the dis-
 310 tribution of α obtained by regression of R against T in the individual integrations is
 311 $1.38 \pm 0.08 \text{ W m}^{-2} \text{ K}^{-1}$ (mean and standard deviation). This is consistent with the
 312 median of $1.43 \text{ W m}^{-2} \text{ K}^{-1}$ estimated by Dessler et al (2018) from the same dataset
 313 using differences between the means of the last and the first decades (Equation 2). The
 314 standard deviation of slopes from the difference method is $0.14 \text{ W m}^{-2} \text{ K}^{-1}$, larger
 315 than from the regression method, because the latter uses more data, making it a more
 316 efficient estimator (Appendix D.1).

317 The choice of T as independent variable follows our physical intuition that T deter-
 318 mines the magnitude of R rather than vice-versa. Using the *historical* MPI-ESM1.1 en-
 319 semble, we show that this choice is preferable also on statistical grounds (Appendix B).
 320 We show further that estimates of historical α made by OLS regression from real-world
 321 R and T are biased low, giving an overestimate of historical EffCS, due to noise T' in
 322 T which does not produce proportionate variability $\alpha T'$ in R (Appendix C).

323 Evaluating the statistics for all the AOGCMs, we find that the bias is larger in
 324 $\tilde{\alpha}$ (multimodel mean of 20%) for a 30-year period than in $\bar{\alpha}$ (10%) for the entire
 325 historical period. The bias affects the difference method as well as OLS regression
 326 (Appendix D.1). Total least-squares regression is a method that would avoid the bias,
 327 but it is not obviously applicable because it depends on information that we do not
 328 have (Appendix D.5).

329 As well as the mean bias, individual integrations give a spread of slopes due to the
 330 noise. The consequent uncertainty is larger in $\tilde{\alpha}$ than in $\bar{\alpha}$ (multimodel mean respec-
 331 tively of $0.42 \text{ W m}^{-2} \text{ K}^{-1}$ or $\sim 30\%$, and $0.11 \text{ W m}^{-2} \text{ K}^{-1}$ or $\sim 10\%$, Appendix C).

332 For the real world, random error in the observational dataset, due to instrumental
 333 uncertainty or sampling, is a possible source of noise in T that is uncorrelated with R ,
 334 but this is not relevant to the model world, where we have perfect information. In both
 335 worlds, unforced variability in the climate system, unrelated to F , is the likely source
 336 of bias, through two physical mechanisms (both demonstrated in Appendix D.6).

337 First, if variability is driven by spontaneous fluctuations in N that have some
 338 persistence, and if the response in T to these fluctuations has some thermal inertia,
 339 α will be biased low (the second case considered by Proistosescu et al 2018). This
 340 effect could be caused for example by interannual variability in cloudiness, and hence
 341 planetary albedo, produced by regional climate variability; such variations may persist
 342 with anomalies of SST, and the heat capacity of the upper ocean sets the timescale of
 343 response. The effect causes α to be underestimated by OLS because the spontaneous
 344 fluctuation in N is misattributed to R .

345 Second, if spontaneous variability in SST produces a response in N with a different
 346 α from the externally forced response, probably because it has a different geographical
 347 pattern (Dessler et al 2018), the OLS slope is contaminated by α from the variability.
 348 Unlike the first mechanism, this one can produce variability in α in either sense.

349 5 Time-variation of historical climate feedback related to forcing agents

350 The original motivation for estimating ECS from historical climate change depends on
 351 the assumption that α is constant. If it is not, the historical α may differ from α for
 352 idealised CO_2 -forced climate change (Paynter and Frölicher 2015). In this section, we
 353 examine the dependence of α in AOGCMs on time, and relate this to the changing
 354 nature of the forcing, in order to work out how CO_2 α may best be estimated from
 355 historical α .

356 The relationship between forcing and climate response is often discussed in terms
 357 of the efficacy, defined as T forced by unit F of the given agent divided by T for
 358 unit forcing of CO_2 (Hansen et al 2005). Our discussion is related to this concept,
 359 but it is framed in terms of α because we are interested in the variation of R with T
 360 due to climate feedbacks. In contrast, efficacy quantifies the dependence of T on F ,
 361 which involves ocean heat uptake as well, and its definition therefore requires a choice
 362 of scenario and timescale for the temperature response. For example, efficacy may be
 363 defined using T after a specified elapsed time in an AOGCM experiment with constant
 364 forcing (as by Hansen et al 2005) or the equilibrium T under constant forcing of an
 365 AGCM with a slab ocean.

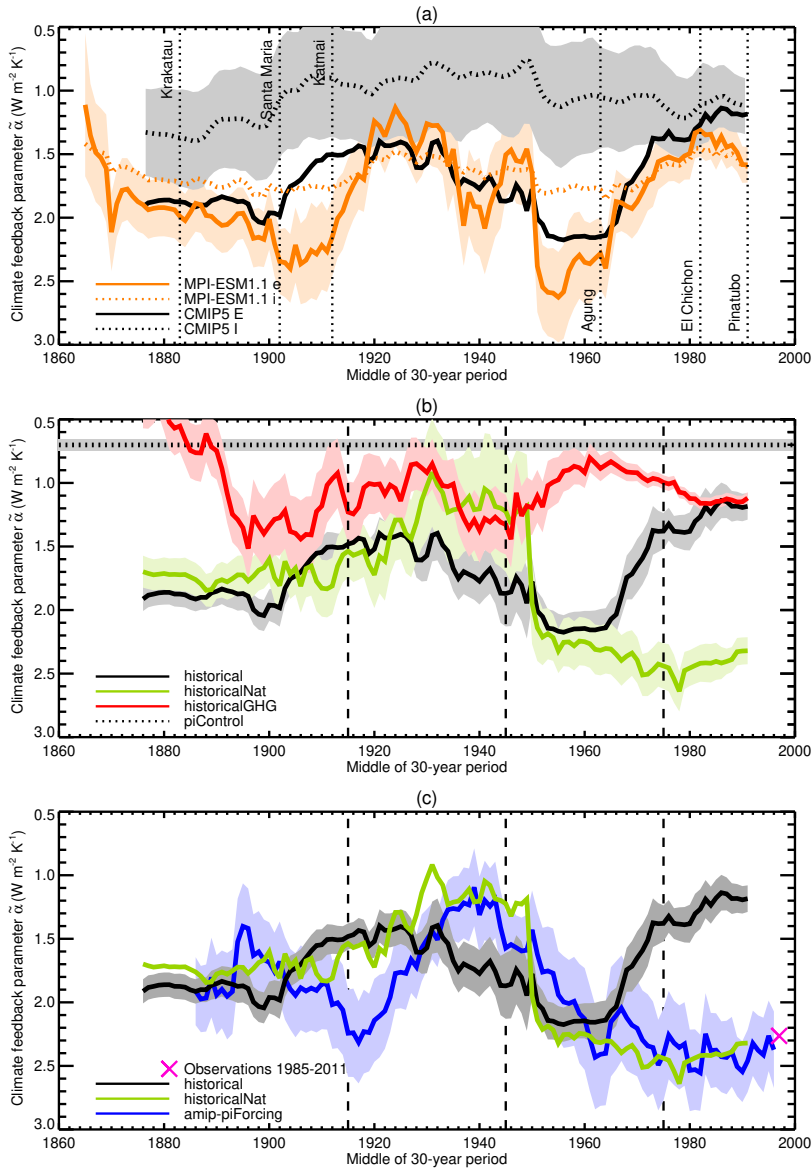


Fig. 5 Time-dependent climate feedback parameter $\tilde{\alpha}_E$ (the same solid black line in all panels, labelled “CMIP5 E” in panel (a) and “historical” in the other two) for the multimodel mean of the CMIP5 *historical* experiment, (a) compared with the mean $\tilde{\alpha}_I$ of individual CMIP5 models (labelled “CMIP5 I”), and with $\tilde{\alpha}_e$ and $\tilde{\alpha}_i$ from the MPI-ESM1.1 ensemble, (b) compared with $\tilde{\alpha}_E$ for the multimodel means of the CMIP5 *historicalGHG* and *historicalNat* experiments, and with the time-mean (dotted horizontal line) of $\tilde{\alpha}$ for 30-year periods in the CMIP5 *piControl* simulations, (c) compared with $\tilde{\alpha}_E$ for the multimodel means of the AGCM *amip-piForcing* the CMIP5 *historicalNat* experiments, and an estimate made from observational datasets for N and T . The lightly coloured regions around the some of the lines are ± 1 standard error, with ± 1 standard deviation for CMIP5 I in (a). In (b) and (c) the vertical dashed lines indicate the beginning of the three periods of the regression analysis of Figure 6a, centred on 1930, 1960 and 1990. Note that $\tilde{\alpha}$ decreases upwards on the vertical axis, in order that the effective climate sensitivity increases upwards.

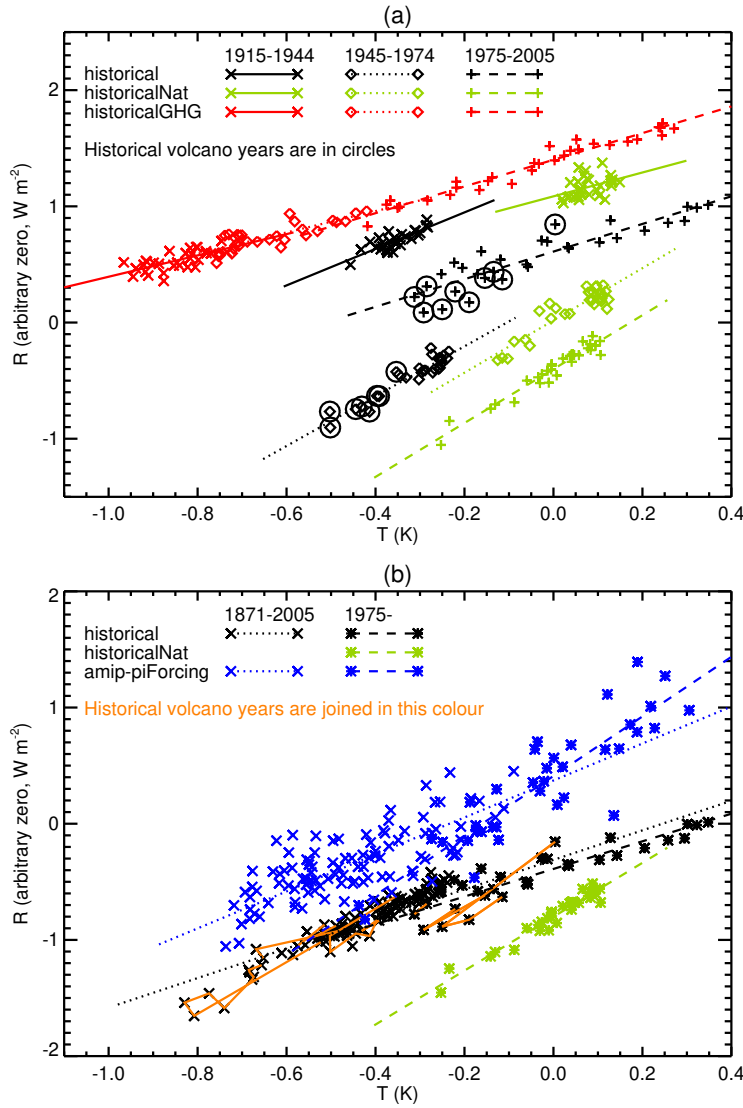


Fig. 6 Regression of annual-mean $R = F - N$ against T (a) for the CMIP5 AOGCM means in *historical*, *historicalGHG* and *historicalNat* experiments in three consecutive periods, centred on 1930, 1960 and 1990, (b) for the CMIP5 AOGCM means in the *historical* and *historicalNat* experiments and the AGCM mean in the *amip-piForcing* experiment, for the entire historical period and for 1975 onwards (to 2005 for CMIP5, 2011 for *amip-piForcing*). The periods are distinguished by the choice of symbol for the data points and the style of line for the regression slope. For the *historical* experiment, the circles mark the years with volcanic ERF $< -0.2 \text{ W m}^{-2}$ in (a), and sequences of such years are joined by a solid line in (b). The same T -axis is used for all experiments and periods, relative to time-mean of 1979–2005 *i.e.* the AMIP period omitting 2006–2008, because the CMIP5 historical period ends in 2005. On the R -axis the experiments are shifted so that they can be seen separately and their slopes compared conveniently, and in (a) the individual periods of *historical* and *historicalNat* are also shifted for the same reason.

366 5.1 Time-variation of climate feedback in the *historical* experiment

367 Using the AOGCM *historical* experiments, we evaluate the time-variation of $\tilde{\alpha}_i(t)$ and
 368 $\tilde{\alpha}_e(t)$ by regression in overlapping 30-year periods *e.g.* $\tilde{\alpha}$ for the 30 years centred on 1st
 369 January 1940 is obtained from regression of annual means for 1925–1954. In the MPI-
 370 ESM1.1 *historical* ensemble, $\tilde{\alpha}_e(t)$ shows significant decadal variation (solid orange
 371 line in Figure 5a). For example, $\tilde{\alpha}_e = 1.14 \pm 0.30 \text{ W m}^{-2} \text{ K}^{-1}$ in 1924 and $2.63 \pm$
 372 $0.36 \text{ W m}^{-2} \text{ K}^{-1}$ in 1955, whose difference of $1.49 \pm 0.47 \text{ W m}^{-2} \text{ K}^{-1}$ is significant at
 373 the 1% level. This variation must be evidence of time-dependence which is synchronous
 374 across the ensemble of integrations, and therefore attributable to external forcing.

375 On the other hand, $\tilde{\alpha}_i(t)$ does not depend significantly on time (dotted orange line
 376 in Figure 5a), judged by comparison with its standard deviation of $0.35 \text{ W m}^{-2} \text{ K}^{-1}$
 377 due to unforced variability (the standard deviation among the 100 integrations, pooled
 378 over years, not shown). This is because unforced variability has a greater effect on
 379 individual integrations, and obscures the response to forcing that can be discerned in
 380 the ensemble mean.

381 Since the *historical* ensembles with CMIP5 models are much smaller than the MPI-
 382 ESM1.1 ensemble, to suppress the unforced variability we aggregate the models, by
 383 calculating a time-dependent climate feedback parameter, denoted by $\tilde{\alpha}_E$ (Table 1),
 384 from the multimodel-mean $R(t)$ and $T(t)$ of the ensemble means of individual CMIP5
 385 models *i.e.* treating the models as equally weighted members of a “super-ensemble”.
 386 (We use the word “multimodel” instead of just “model” to emphasise that it is a
 387 mean over *all* models, rather than the mean over all integrations of a *single* model.)
 388 We assume that the forced response will have correlated time-dependence among the
 389 models, whereas the unforced variability will be uncorrelated. The multimodel mean is
 390 used for similar reasons in statistical studies of attribution of climate change to forcing
 391 agents (*e.g.* Jones et al 2013; Hua et al 2018).

392 The small standard error of $\tilde{\alpha}_E$ (grey envelope in Figure 5b) means that its time-
 393 variation is well-defined and statistically significant. It is moreover rather similar to
 394 $\tilde{\alpha}_e$ of MPI-ESM1.1 (compare solid black and orange lines in Figure 5a), corroborating
 395 the idea that the time-variation is forced, and thus similar among all models. There
 396 is a minimum in $\tilde{\alpha}_E$ around 1930, a maximum during 1945–1974, and the absolute
 397 minimum (highest EffCS) occurs after 1980. The time-variation cannot be an artefact
 398 arising from the OLS bias because the minima in $\tilde{\alpha}$ occur when the rate of warming
 399 is largest (around 1930 and after 1980), and hence the bias towards small $\tilde{\alpha}$ due to
 400 unforced variability is of minimal importance compared with the response to forcing.

401 The time-variation of $\tilde{\alpha}_E$ in the CMIP5 *historical* experiment is similar in amplitude
 402 and period to the time-variation of $\tilde{\alpha}$ in the AGCM *amip-piForcing* experiment with
 403 observed historical sea-surface temperature (described in Section 1; Andrews et al
 404 2018), but different in time-profile (compare black and blue lines in Figure 5c). We will
 405 study *amip-piForcing* in Section 6, once we have drawn conclusions from the present
 406 section concerning the response to forcing in the AOGCMs.

407 For comparison, we also calculate a multimodel mean, denoted by $\tilde{\alpha}_I(t)$ (dotted
 408 black line in in Figure 5a), from the $\tilde{\alpha}_i(t)$ timeseries of the individual models. Like $\tilde{\alpha}_i$
 409 of MPI-ESM1.1, $\tilde{\alpha}_I$ has insignificant forced time-variation, judged by comparison with
 410 the standard deviation among integrations (grey envelope, calculated for each model
 411 ensemble and pooled over models; if also pooled over years, the standard deviation is
 412 $0.42 \text{ W m}^{-2} \text{ K}^{-1}$). The lack of significant forced variation is due to the dominance of $\tilde{\alpha}$
 413 by unforced variability in individual integrations, while the greater OLS bias (Section 4)

414 caused by larger unforced variability explains why $\tilde{\alpha}_I < \tilde{\alpha}_E$ at all times (compare solid
415 and dotted black lines in Figure 5a).

416 5.2 Greenhouse-gas forcing

417 Since the largest historical forcing is CO₂, we consider the possibility that the response
418 to CO₂ could somehow cause forced time-variation in $\tilde{\alpha}_E$. Most CMIP5 models have
419 a tendency for α to decrease with time under constant CO₂ (Armour et al 2013;
420 Andrews et al 2015). In our set of CMIP5 AOGCMs, regression of $-N$ against T for
421 years 1–20 and years 1–140 of *abrupt4xCO2* gives multimodel-mean $\alpha = 1.26$ and
422 $1.02 \text{ W m}^{-2} \text{ K}^{-1}$ respectively. In some AGCMs and AOGCMs, it has been found that
423 α decreases as CO₂ concentration rises (Good et al 2012; Jonko et al 2012; Gregory
424 et al 2015). Either of these effects might explain the long-term decreasing tendency in
425 *historical* $\tilde{\alpha}_E$ (Figure 5b), although not its decadal variation.

426 To test this hypothesis, we calculate $\bar{\alpha}_E$ in the *historicalGHG* experiment, whose
427 forcing is predominantly CO₂, using the AR5 estimate of greenhouse-gas $F(t)$. We find
428 that R and T in *historicalGHG* have a high correlation coefficient of 0.99 over the
429 historical period (1871–2005, shown in red in Figure 6a for the period since 1915), and
430 there is little time-variation in $\tilde{\alpha}_E$ in the *historicalGHG* experiment (solid red line in
431 Figure 5b). Therefore we reject the hypothesis that the long-term decreasing trend in
432 *historical* $\tilde{\alpha}_E$ is due to CO₂ forcing. After about 1960, *historical* $\tilde{\alpha}_E$ *decreases* strongly,
433 This tendency is opposite to that of *historicalGHG* $\tilde{\alpha}_E$, which *increases* slightly, per-
434 haps due to reduction of OLS bias as the greenhouse-gas forcing grows relative to the
435 unforced variability (Appendices D.3 and D.6).

436 5.3 Comparison of *historicalGHG* and *abrupt4xCO2* climate feedback

437 The *historicalGHG* $\bar{\alpha}_E = 1.03 \pm 0.01 \text{ W m}^{-2} \text{ K}^{-1}$ (EffCS 3.6 K, Figure 6a) is close
438 to multimodel-mean $\alpha = 1.02 \text{ W m}^{-2} \text{ K}^{-1}$ from years 1–140 of *abrupt4xCO2* (Sec-
439 tion 5.2). The correlation coefficient across models between *abrupt4xCO2* α and *his-*
440 *toricalGHG* $\bar{\alpha}_e$ is 0.55 for years 1–20 and 0.68 for years 1–140, both significant at
441 the 10% level. This similarity is expected, since *historicalGHG* is dominated by CO₂
442 forcing, but because CO₂ α varies with time and perhaps with CO₂ concentration,
443 and α might differ among the various greenhouse gases, we cannot expect a perfect
444 correlation. We suppose that it is larger for years 1–140 because this timescale is more
445 similar to the length of the *historicalGHG* experiment.

446 The correlation might also be reduced by our neglect of model-dependence in the
447 greenhouse-gas $F(t)$, which we do not know for any of the models. To take this approx-
448 imately into account, we recalculate *historicalGHG* $\bar{\alpha}_e$ using the AR5 greenhouse-gas
449 F scaled for each AOGCM by the ratio of that AOGCM’s *abrupt4xCO2* ERF to the
450 multimodel-mean value. The correlation coefficients with *abrupt4xCO2* α are increased
451 to 0.61 for years 1–20 and 0.77 for years 1–140 (Figure 7a), supporting the conjecture
452 that the model spread in greenhouse-gas forcing is substantial (Andrews et al 2012;
453 Chung and Soden 2015). The *historicalGHG* $\bar{\alpha}_e$ is about 10% larger than *abrupt4xCO2*
454 α for years 1–140 in the multimodel mean.

 455 5.4 Volcanic and anthropogenic aerosol forcings

456 We have seen that the time-dependence of *historical* $\tilde{\alpha}_E$ is statistically significant
 457 (Section 5.1), but not related to greenhouse-gas forcing (Section 5.2). Therefore we
 458 suppose that it is due to the varying relative importance of the other forcing agents.
 459 Such an effect could occur if α depends on the nature of the forcing. As discussed at
 460 the start of Section 5, this idea is related to the efficacy of forcing agents. For many
 461 agents, including anthropogenic aerosols, α is found to be close to CO₂ α (efficacy is
 462 near unity), provided ERF is used to quantify forcing (Hansen et al 2002; Shine et al
 463 2003; Sherwood et al 2015). For volcanic aerosol, α may be larger than for CO₂ (EffCS
 464 smaller, efficacy less than unity; Marvel et al 2016; Gregory et al 2016; Ceppi and
 465 Gregory in press).

466 In this discussion, we frequently consider and contrast three consecutive historical
 467 periods, which have different mixtures of forcing, as described in the following para-
 468 graphs. We choose them each to be 30 years, like the sliding window used to evaluate
 469 $\tilde{\alpha}$, because that means the OLS bias will not affect their comparison (Section 4).

470 The time-dependence of $\tilde{\alpha}_E$ in *historicalNat*, in which the forcing is dominated by
 471 volcanic aerosol (Figure 1), shows large decadal variation (Figure 5b). During 1915–
 472 1944 there were no large volcanic eruptions, so the variation of T and R and their
 473 correlation of 0.41 are all relatively small (green crosses in Figure 6a) and must be due
 474 nearly entirely to unforced variability. For *historicalNat* during this period regression
 475 gives $\tilde{\alpha}_E = 0.7 \pm 0.4 \text{ W m}^{-2} \text{ K}^{-1}$ (solid green line), which is not distinguishable from
 476 *historicalGHG* $\tilde{\alpha}_E = 1.0 \text{ W m}^{-2} \text{ K}^{-1}$ (solid red line, Section 5.2).

477 Unlike in *historicalNat*, T and R have substantial trends in the *historical* experi-
 478 ment during 1915–1944 (black crosses in Figure 6a) due to anthropogenic forcing, es-
 479 pecially by greenhouse gases (Figure 1). The *historical* $\tilde{\alpha}_E = 1.4 \pm 0.1 \text{ W m}^{-2} \text{ K}^{-1}$ of
 480 this period (solid black line) is somewhat larger than for greenhouse gas forcing (solid
 481 red line). This could be explained by the growth of negative anthropogenic aerosol
 482 forcing during this period, with a smaller α (larger EffCS) than for greenhouse-gas
 483 forcing; the combination would produce a larger α than either alone (Appendix B in
 484 supplementary online material of Gregory and Andrews 2016).

485 For *historicalNat* for the period since 1945, during which there were three large
 486 volcanic eruptions, $\tilde{\alpha}_E$ is fairly constant (green line in Figure 5b). The regression of R
 487 against T gives $\alpha = 2.5 \pm 0.2 \text{ W m}^{-2} \text{ K}^{-1}$ for 1945–1974 and $2.4 \pm 0.1 \text{ W m}^{-2} \text{ K}^{-1}$ for
 488 1975 onwards, which are very similar (EffCS 1.5 K), and more than twice *historicalGHG*
 489 $\tilde{\alpha}_E$ (compare the dotted and dashed red lines in Figure 6a with the dotted and dashed
 490 green lines). These results suggest that the climate feedback parameter for volcanic
 491 forcing is larger (smaller EffCS) than for greenhouse gases (predominantly CO₂) in
 492 CMIP5 AOGCMs on average.

493 For 1945–1974 (30 years centred on 1st January 1960) *historical* $\tilde{\alpha}_E = 2.1 \pm 0.2$
 494 $\text{W m}^{-2} \text{ K}^{-1}$, similar to *historicalNat* (dotted black and green lines in Figure 6a), and
 495 distinct from *historicalGHG* (dotted red line). We suggest that *historical* and *histori-*
 496 *calNat* $\tilde{\alpha}_E$ are similar during this period because the increase in greenhouse-gas forcing
 497 in the *historical* experiment is offset by the increase in negative anthropogenic aerosol
 498 forcing, leaving only a small net anthropogenic forcing trend (Figure 1), so the strong
 499 volcanic forcing from Agung is the greatest influence in both experiments.

500 For 1975–2005 (a period of 31 years, centred in 1990 and running up to the end
 501 of the CMIP5 historical integrations), *historical* $\tilde{\alpha}_E = 1.2 \pm 0.1 \text{ W m}^{-2} \text{ K}^{-1}$ diverges
 502 from *historicalNat* and comes much closer to *historicalGHG* (black approaches red in

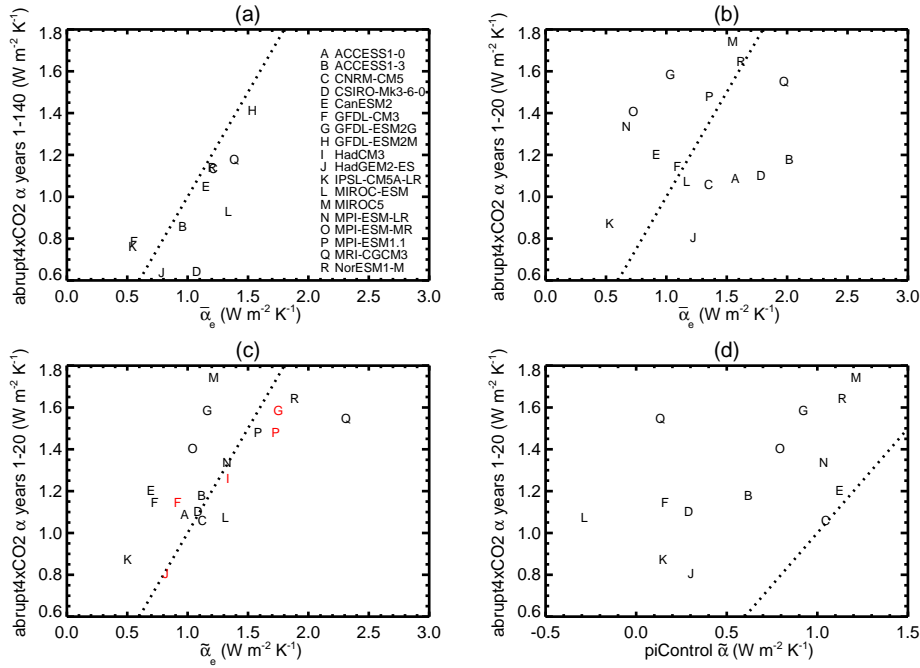


Fig. 7 Relationships in CMIP5 AOGCMs between $abrupt4xCO2 \alpha$ and (a) *historicalGHG* $\bar{\alpha}_e$, (b) *historical* $\bar{\alpha}_e$, (c) *historical* $\bar{\alpha}_e$ for 1975–2004 (in black), *amip-piForcing* $\bar{\alpha}_e$ for 1925–1954 (in red), (d) time-mean *piControl* $\bar{\alpha}$. In (a) we plot α for years 1–140 of *abrupt4xCO2*, and in (b,c,d) years 1–20. In (a) we use the AR5 estimate for *historicalGHG* $F(t)$, scaled for each AOGCM by its own *abrupt4xCO2* ERF (as discussed in the text), and for (b,c) we use our AR5’ estimate for *historical* $F(t)$ for all AOGCMs except HadGEM2-ES and MPI-ESM1.1 (models J and P), for which we use $F(t)$ diagnosed in these models individually (compared in Figure 1). The dotted line in all panels is 1:1; all models lie to the left of this line in (d), indicating that *piControl* $\bar{\alpha} < abrupt4xCO2 \alpha$.

503 Figure 5b, dashed black and red lines have a similar slope in Figure 6a). We suggest
 504 that the *historical* and *historicalGHG* $\bar{\alpha}_E$ are similar during this period because the net
 505 anthropogenic forcing grows much more rapidly due to greenhouse gas increase, once
 506 the aerosol forcing is steady (Figure 1). Despite the further years of volcanic forcing
 507 from El Chichon and Pinatubo, the greenhouse-gas forcing dominates the *historical* F
 508 and the consequent rise in T (Figure 3).

509 In summary, the time-variation of *historical* $\bar{\alpha}_E$ in CMIP5 can be mainly explained
 510 by the varying importance of forcings due to greenhouse gases and volcanic aerosol, if
 511 α is larger for the latter. This means the EffCS is higher (α smaller) when volcanic
 512 forcing is relatively less important, around 1940 (when there were no major eruptions)
 513 and since 1975 (when greenhouse-gas forcing has rapidly increased). The growth of
 514 negative anthropogenic aerosol forcing during the intermediate period meant that the
 515 increase in net anthropogenic forcing was less important than the volcanic forcing, so
 516 the EffCS was dominated by response to volcanic forcing, and was relatively low. This
 517 explanation does not require EffCS for anthropogenic aerosol to differ substantially
 518 from the CO_2 EffCS.

519 5.5 Comparison of *historical* and *abrupt4xCO2* climate feedback

520 Despite the large time-variation of α_E (black in Figure 5), multimodel-mean R and T
 521 are highly correlated (coefficient of 0.94 for 1871–2006, black symbols in Figure 6b).
 522 Moreover, $\bar{\alpha}_E = 1.27 \pm 0.04 \text{ W m}^{-2} \text{ K}^{-1}$ for the entire historical period (dotted black
 523 line in Figure 6b) is very close to the multimodel-mean $\alpha = 1.26 \text{ W m}^{-2} \text{ K}^{-1}$ for years
 524 1–20 of *abrupt4xCO2* (Section 5.2).

525 However, for individual AOGCMs, the correlation of $\bar{\alpha}_e$ with *abrupt4xCO2* α is
 526 much weaker, and insignificant at the 10% level, at 0.24 for years 1–20 (Figure 7b) and
 527 -0.02 for years 1–140. The multimodel standard deviation of the difference between
 528 $\bar{\alpha}_e$ and *abrupt4xCO2* α is 37% ($0.47 \text{ W m}^{-2} \text{ K}^{-1}$). The likely reason is the large
 529 AOGCM spread in F , which we have estimated as $\pm 45\%$ (Section 3.2), due principally
 530 to anthropogenic aerosol. Scaling the greenhouse-gas forcing using the ratio of *abrupt-*
 531 *4xCO2* ERF, as we did for *historicalGHG*, raises the correlation coefficients somewhat,
 532 to 0.37 and 0.24, but they are still insignificant at the 10% level, confirming the
 533 dominant effect of uncertainty in non-greenhouse-gas forcing.

534 A more accurate estimate might be obtained from periods which are dominated by
 535 CO_2 forcing, when *historical* $\tilde{\alpha}$ should be closer to CO_2 α and F is more accurately
 536 known. One possibility is the recent decades, when the greenhouse-gas forcing has
 537 been increasing rapidly and the anthropogenic sulphate aerosol forcing has been fairly
 538 constant (Section 5.4; Gregory and Forster 2008; Bengtsson and Schwartz 2013), so
 539 *historical* and *historicalGHG* $\tilde{\alpha}_E$ are consequently close (Figure 5b). For 1975–2004
 540 (30 years centred on 1st January 1990) the correlation of $\tilde{\alpha}_e$ with *abrupt4xCO2* α is
 541 0.64 (Figure 7c), a considerably stronger correlation than for $\bar{\alpha}_e$, and the standard
 542 deviation of the difference is smaller, at 27%. Scaling the greenhouse-gas forcing using
 543 the ratio of *abrupt4xCO2* ERF improves the correlation only a little in this case.

544 For most of the historical period, $\tilde{\alpha}_E(t)$ is much larger (EffCS smaller) in *histori-*
 545 *cal* than *historicalGHG* (the time-mean difference between the black and red lines is
 546 $0.75 \text{ W m}^{-2} \text{ K}^{-1}$ in Figure 5b), but the multimodel-mean difference between *historical*
 547 $\bar{\alpha}_e$ and *abrupt4xCO2* α is only 2% ($0.03 \text{ W m}^{-2} \text{ K}^{-1}$). We can understand this ap-
 548 parent contradiction by considering multimodel-mean $R(t)$ and $T(t)$. The slope during
 549 intervals of volcanic forcing (joined by solid orange lines in Figure 6b) is evidently
 550 greater than at other times, consistent with time-varying *historical* $\tilde{\alpha}_E(t)$ (Figure 5b).
 551 However, the volcanic forcing is small on the long-term mean, and although the periods
 552 affected by volcanic forcing are of several years, they are only temporary digressions
 553 from the long-term trend. Hence the large volcanic $\tilde{\alpha}$ has little effect on the best-fit
 554 slope for the entire historical period (dotted black line in Figure 6b), which is only a
 555 little larger than $\tilde{\alpha}_E = 1.19 \pm 0.10 \text{ W m}^{-2} \text{ K}^{-1}$ for the last 30 years of the timeseries
 556 (dashed black line, the same as in Figure 6a).

557 In summary, in the AOGCMs, as an estimate of *abrupt4xCO2* α , *historical* $\bar{\alpha}_E$ has a
 558 small positive bias, because of the influence of volcanic forcing, and a large uncertainty,
 559 due principally to anthropogenic aerosol forcing. In the real world, we cannot evaluate
 560 $\bar{\alpha}$ accurately because we do not have adequate estimates of F and N for the entire
 561 historical period. Response to volcanic forcing has a much stronger effect on the time-
 562 dependent $\tilde{\alpha}_E$ than it does on $\bar{\alpha}_E$. Therefore $\tilde{\alpha}_E$ from periods that are affected by
 563 volcanoes has a large positive bias as an estimate of *abrupt4xCO2* α . In the AOGCMs,
 564 the bias is smallest in the period since 1975, during which we have the best observations
 565 of the real world.

566 5.6 Comparison of unforced and *abrupt4xCO2* climate feedback

567 In Section 5.4 we noted that *historicalNat* $\tilde{\alpha}_E$ and *historicalGHG* $\tilde{\alpha}_E$ for 1915–1944
 568 are not distinguishable. Since there are no volcanic eruptions during this period, *his-*
 569 *toricalNat* has no forcing. Therefore it is of interest to know what $\tilde{\alpha}$ to expect from
 570 unforced variability alone, which we evaluate from the *piControl* experiments by re-
 571 gressing R ($= -N$ since $F = 0$) against T in overlapping 30-year segments. We use
 572 480 ($= 16 \times 30$) years from each AOGCM, and exclude ACCESS1.0, for which we have
 573 only 250 years.

574 For the population of $\tilde{\alpha}$, taking all segments from all models together, the mean
 575 $\tilde{\alpha} = 0.70$ (dotted horizontal line in Figure 5b). Neglecting autocorrelation for lags
 576 greater than 30 years, the population contains 16 independent values from each of 15
 577 experiments. The population standard deviation is $0.69 \text{ W m}^{-2} \text{ K}^{-1}$, so the standard
 578 error of the time-mean $\tilde{\alpha}_E$ is $0.69/\sqrt{16 \times 15} = 0.044 \text{ W m}^{-2} \text{ K}^{-1}$ (grey envelope around
 579 the dotted horizontal line). Hence *historical* $\tilde{\alpha}_E(t)$ is always distinct from time-mean
 580 *piControl* $\tilde{\alpha}$.

581 *HistoricalGHG* and *piControl* are different in the character of the covariation of R
 582 and T , which is highly correlated in the former but not in the latter (correlation coeffi-
 583 cient of 0.24 between annual-mean R and T in the *piControl* population). Nonetheless,
 584 their regression slopes are similar. Although *historicalGHG* $\tilde{\alpha}_E$ is greater than *pi-*
 585 *Control* $\tilde{\alpha}$ during nearly all the historical period, their difference is rarely statistically
 586 significant (Figure 5b, 5% two-tailed significance level) before about 1970. This explains
 587 the similarity of *historicalNat* and *historicalGHG* $\tilde{\alpha}_E$ during 1915–1945.

588 For each model we compare the *piControl* $\tilde{\alpha}$ for unforced variability with *abrupt-*
 589 *4xCO2* α for CO_2 forcing. These quantities have a modest but significant correlation
 590 across models (0.55, Figure 7d), as found by Zhou et al (2015) for the cloud component.
 591 Colman and Power (2018) note both similarities and differences in feedbacks for decadal
 592 variability and CO_2 forcing. It is clear that *abrupt4xCO2* α is larger than *piControl* $\tilde{\alpha}$
 593 in all models, leading us to infer that *historicalGHG* $\tilde{\alpha}_e$ and $\tilde{\alpha}_E$ are also larger than
 594 *piControl*. In some models, *piControl* $\tilde{\alpha} < 0.5 \text{ W m}^{-2} \text{ K}^{-1}$, implying EffCS exceeding
 595 7 K, and it is negative in one model (MIROC5). Dessler (2013) found similar results for
 596 *piControl* experiments of AOGCMs from the Coupled Model Intercomparison Project
 597 Phase 3 (CMIP3). These low values result from a pronounced OLS bias due to noise
 598 in T that is not correlated with R (Section C). There is a more complex relationship
 599 between R and T for internally generated fluctuations, and it is physically incorrect to
 600 treat R simply as an instantaneous response to T (Xie and Kosaka 2017; Lutsko and
 601 Takahashi 2018; Proistosescu et al 2018)

602 **6 Time-variation of historical climate feedback related to SST patterns**

603 Previously published work has shown that the variation of α is mostly determined
 604 by the pattern and magnitude of sea surface change in response to radiative forcing
 605 (Armour et al 2013; Andrews et al 2015; Gregory and Andrews 2016; Haugstad et al
 606 2017; Ceppi and Gregory in press). The effect of the agent comes mainly via the
 607 surface forcing, which is rapidly modified by climate feedbacks, ocean heat uptake and
 608 atmospheric and oceanic dynamical responses. We depend on AOGCMs to project the
 609 consequent sea surface changes, but we do not know whether their results are realistic
 610 in the characteristics relevant to α .

611 In this section we compare α from historical AOGCM simulations, driven by forcing
 612 agents, with α from AGCM simulations driven by sea surface conditions prescribed
 613 from observations. AMIP experiments have shown that AGCMs reproduce the time-
 614 variation of TOA radiation and other quantities quite well when given realistic surface
 615 conditions (Allan et al 2014). Thus the advantage of the AGCM simulations is their
 616 closer resemblance than the AOGCM simulations to the real historical record, while
 617 their disadvantage is that they do not allow us to isolate the effects of the individual
 618 forcing agents and unforced variability, which have imprinted their effects all together
 619 on the observational sea surface conditions.

620 6.1 Time-variation of climate feedback in the *amip-piForcing* experiment

621 The AGCM experiment named *amip-piForcing*, using observationally derived time-
 622 dependent historical sea-surface boundary conditions from the Atmosphere Model Inter-
 623 comparison Project (AMIP, Gates et al 1999; Hurrell et al 2008), with constant
 624 pre-industrial forcing agents (atmospheric composition etc.), has recently been carried
 625 out with various AGCMs (Andrews 2014; Gregory and Andrews 2016; Zhou et al
 626 2016; Silvers et al 2018; Andrews et al 2018). In this experiment, $F = 0 \Rightarrow R =$
 627 $-N = \alpha T$. Because *amip-piForcing* does not have time-varying forcing agents, the
 628 evaluation of its $\bar{\alpha}_e$ is not affected by the uncertainty in anthropogenic aerosol ERF,
 629 unlike the CMIP5 *historical* $\bar{\alpha}_e$. In this section we use the *amip-piForcing* ensembles
 630 of ECHAM6.3, HadGEM2-A, GFDL-AM2.1 and GFDL-AM3 (the AGCMs of MPI-
 631 ESM1.1, HadGEM2-ES, GFDL-ESM2M and GFDL-CM3; data from Andrews et al
 632 2018) and HadCM3-A (the AGCM of HadCM3, Gordon et al 2000, employed for fur-
 633 ther experiments in this section). The *amip-piForcing* experiment is included in the
 634 Cloud Feedback Model Intercomparison Project of CMIP6 (Webb et al 2017).

635 In each of these AGCMs, $\bar{\alpha}_e$ obtained by regression of $-N$ against T from *amip-*
 636 *piForcing* for the entire historical period is larger (EffCS smaller) than in the *abrupt-*
 637 *4xCO2* experiment with the corresponding AOGCM (Andrews et al 2018). Regression
 638 of multimodel-mean R against T for the five AGCMs gives $\bar{\alpha}_E = 1.59 \pm 0.08 \text{ W m}^{-2} \text{ K}^{-1}$
 639 for *amip-piForcing* (blue crosses and dotted line in Figure 6b), about 30% larger than
 640 both *historical* $\tilde{\alpha}_E$ (black crosses and dotted line), and multimodel mean *abrupt4xCO2*
 641 $\alpha = 1.25 \text{ W m}^{-2} \text{ K}^{-1}$ for years 1–20 (Section 5.5).

642 When computed in a 30-year window, $\tilde{\alpha}(t)$ shows large decadal variation, but the
 643 spread of $\tilde{\alpha}$ among the integrations of each AGCM is rather small, because most of
 644 the interannual variability is prescribed through the sea surface conditions (Gregory
 645 and Andrews 2016, who show as well that SST patterns dominate the effect, and sea
 646 ice variations are relatively unimportant). In each AGCM, there is consequently little
 647 difference between $\tilde{\alpha}_i(t)$ and $\tilde{\alpha}_e(t)$, unlike in AOGCMs. Owing to the strong influence of
 648 the common surface boundary conditions, the AGCMs furthermore have synchronised
 649 time-variations in $\tilde{\alpha}$ (Andrews et al 2018), illustrated by $\tilde{\alpha}_E$ of the multimodel mean
 650 (blue in Figure 5c), but they have different time-means and vary with roughly constant
 651 offsets. Their spread is similar to that of α in the standard idealised *amip-p4K* AGCM
 652 experiment, which imposes a uniform SST warming of 4 K (Ringer et al 2014).

653 The minimum $\tilde{\alpha}_E$ (maximum EffCS) of *amip-piForcing* is close to *historicalGHG*
 654 $\tilde{\alpha}_E$ ($1.03 \text{ W m}^{-2} \text{ K}^{-1}$, Section 5.5), and occurs in the middle of the longest interval
 655 without major volcanic eruptions, when forced climate change was therefore anthro-
 656 pogenic. This is consistent with the inference that EffCS for greenhouse-gas forcing

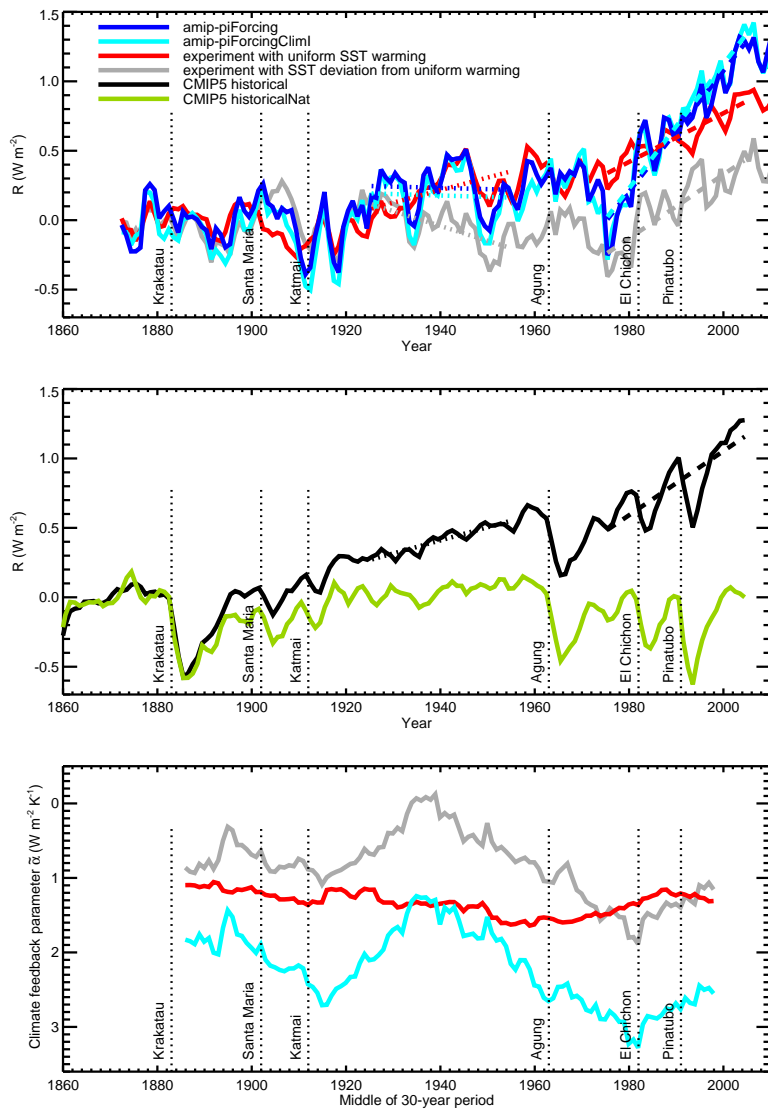


Fig. 8 (a,b) Timeseries of ensemble-mean global-mean radiative response R with respect to the time-mean of 1860–1899 in the HadCM3-A experiments (see text for explanation), CMIP5 *historical* and *historicalNat* experiments. The timeseries have been smoothed by calculating a three-year running mean. Linear regressions for $R(t)$ during 1925–1954 and 1975–2004 are shown by dotted and dashed lines respectively for all experiments except *historicalNat*. (c) Time-dependent climate feedback parameter $\tilde{\alpha}_e$ computed with $R(t)$ from the HadCM3-A experiments indicated and $T(t)$ from HadCM3-A *amip-piForcingClimI*. All panels follow the legend in (a).

657 is higher than for volcanic forcing. For the five AGCMs in our ensemble of *amip-*
 658 *piForcing* experiments, we have compared $\tilde{\alpha}_e$ for 1925–1954 with *abrupt4xCO2* α of
 659 the corresponding AOGCM (red in Figure 7c). The rank correlation is perfect, and
 660 the (product–moment) correlation coefficient is 0.94, consistent with the dominance of
 661 CO₂ forcing during this period.

662 The maximum $\tilde{\alpha}_E$ (minimum EffCS) of *amip-piForcing* is attained in the period
 663 since 1960, during which it is fairly constant, while CMIP5 *historical* $\tilde{\alpha}_E$ is declining
 664 (EffCS increasing), due to the dominance of the greenhouse-gas increase over volcanic
 665 forcing once anthropogenic aerosol has stabilised (as found above, Section 5.4). The
 666 large recent $\tilde{\alpha}_E \simeq 2.5 \text{ W m}^{-2} \text{ K}^{-1}$ of *amip-piForcing* is outside the range of all indi-
 667 vidual CMIP5 *historical* integrations since 1960 (Marvel et al 2018) and of all indi-
 668 vidual CMIP5 *piControl* integrations, whose maximum $\tilde{\alpha}$ are 2.3 and 2.2 $\text{W m}^{-2} \text{ K}^{-1}$
 669 respectively for 30-year periods, and it is about twice the CMIP5 multimodel-mean
 670 *abrupt4xCO2* α (Section 5.5).

671 6.2 Effect of patterns of SST change on radiative response

672 Since *amip-piForcing* and *historical* experiments both reproduce observed $T(t)$ closely,
 673 the differences in $\tilde{\alpha} = dR/dT$ between *amip-piForcing* and *historical*, which are particu-
 674 larly large around 1940 and 1990 (Figure 5c), must be due to differences in $R(t)$. During
 675 1925–1954 (30 years around 1940), $R = F - N$ in the CMIP5 *historical* multimodel
 676 mean has an increasing trend, but $R = -N$ in the HadCM3-A *amip-piForcing* experi-
 677 ment has no trend (black in Figure 8b and blue in Figure 8a respectively), consistent
 678 with $\tilde{\alpha}$ being smaller in *amip-piForcing* (EffCS larger). By contrast, during 1974–2004
 679 (30 years around 1990), R is increasing about twice as fast in *amip-piForcing*, which
 680 has larger $\tilde{\alpha}$ (EffCS smaller).

681 To investigate how the two sets of sea surface fields (one from CMIP5 AOGCMs,
 682 the other from observations) produce the same $T(t)$, but different $R(t)$, we use three
 683 further HadCM3-A experiments with constant pre-industrial forcing agents, like *amip-*
 684 *piForcing*. These experiments have no interannual variation in sea ice concentration,
 685 which follows the climatological annual cycle of the AMIP dataset for 1871–1900. The
 686 first of the three is the *amip-piForcingClimI* experiment (Gregory and Andrews 2016),
 687 which has the same SST fields as *amip-piForcing*, and yields very similar $R(t)$ (blue
 688 and cyan in Figure 8a), confirming that the interannual variation is due almost entirely
 689 to SST changes (rather than sea ice changes).

690 The other two experiments follow Zhou et al (2016). One of them applies the global
 691 warming but no change in SST pattern, while the other applies the pattern of change
 692 but no global warming. They aim to distinguish the effects on α from variation of
 693 global-mean T and from the changing pattern of SST. The monthly SST fields for
 694 1871–2012 for both experiments are derived from the AMIP SST fields $T_S(x, y, M, Y)$,
 695 where x, y are longitude and latitude, M the month within the year and Y the year.

696 First we calculate the monthly SST climatology $T_{SC}(x, y, M)$ of the late nineteenth
 697 century (1871–1900), which we treat as the unperturbed climate, then we calculate the
 698 anomaly $\delta T_S = T_S(x, y, M, Y) - T_{SC}(x, y, M)$ of the SST in a given month from
 699 the unperturbed climatological mean. In one experiment, a geographically uniform
 700 warming δT_{SU} is added to the climatological SST, equal to the global-mean of the
 701 anomaly,

$$\delta T_{SU}(x, y, M, Y) = G(\delta T_S(M, Y)),$$

702 where $G(\cdot)$ denotes a global mean. In the other experiment, the local perturbation
 703 δT_{SD} to the climatology is the deviation of the local anomaly from its global mean,

$$\begin{aligned}\delta T_{SD}(x, y, M, Y) &= \delta T_S(x, y, M, Y) - G(\delta T_S(M, Y)) \\ &= \delta T_S(x, y, M, Y) - \delta T_{SU}(x, y, M, Y).\end{aligned}$$

704 By construction,

$$\delta T_{SU} + \delta T_{SD} = \delta T_S$$

705 and

$$G(\delta T_{SD}(M, Y)) = 0.$$

706 In the experiment with the uniform perturbation δT_{SU} , the time-mean global-mean
 707 surface air temperature anomaly is $T = 0.37$ K for 1975–2004 with respect to the
 708 1871–1900 climatology, almost the same as *amip-piForcingClimI*, and 15% less than
 709 $T = 0.44$ K from *amip-piForcing* because of omitting the effect of the recent decline in
 710 Arctic sea-ice.

711 The zero-mean perturbation δT_{SD} to SST produces negligible global-mean temper-
 712 ature change, but the time-varying changes to the pattern of SST have a strong effect
 713 on cloudiness and thus affect N and hence R . During 1975–2004, the trends in R in the
 714 HadCM3-A uniform and deviation experiments are positive ($dR/dT > 0$) and about
 715 the same size (dotted red and grey lines in Figure 8a). Each *alone* is similar to the
 716 trend in the CMIP5 *historical* experiment (dotted black line in Figure 8b), consistent
 717 with our finding above that in *amip-piForcing*, whose SST perturbation is the sum of
 718 the uniform and deviation perturbations, the trend of R is about twice the size as in
 719 the *historical* experiment, making the EffCS smaller in *amip-piForcing*.

720 During 1925–1954, the trends in R in the HadCM3-A uniform and CMIP5 *historical*
 721 experiments are positive and similar, but the R in the HadCM3-A deviation experiment
 722 has a *negative* trend. That is, although global-mean T is rising, the changing pattern
 723 of SST tends to produce an *increasing* trend in heat uptake ($dN/dT > 0$, $dR/dT < 0$)
 724 by the climate system. The opposed trends due to the global mean and its pattern lead
 725 to the weak net trend of R and make the EffCS larger in *amip-piForcing* during this
 726 period.

727 Thus R is not a response to T alone, but depends also on the changing patterns
 728 of SST. It could be that both the global mean and the patterns have the same causes
 729 (unforced or forced), but they do not have a consistent relationship. The time-variation
 730 of $\tilde{\alpha}$ in *amip-piForcingClimI* (and therefore *amip-piForcing*) is mainly due to the pat-
 731 terns of δT_{SD} , while $\tilde{\alpha}$ for the uniform δT_{SU} is fairly constant through the historical
 732 period (Figure 8c). Assuming that HadCM3-A is typical of AGCMs in *amip-piForcing*,
 733 we suppose that the common time-variation of $\tilde{\alpha}$ is due to the patterns, while the fairly
 734 time-constant model spread is due to model-dependent climate feedback in response
 735 to uniform warming.

736 6.3 Differences between simulated and observed responses to volcanic forcing

737 In Section 5.4 we concluded that the time-dependence of *historical* $\tilde{\alpha}_E$ could be mainly
 738 explained by the varying relative importance of forcings due to greenhouse gases and
 739 volcanic aerosol, if α is larger for the latter. In Sections 6.1 and 6.2 we have seen
 740 that the time-variation of $\tilde{\alpha}_E$ is different for *amip-piForcing* and *historical*, due to the

741 changing patterns of deviation of SST from its global mean. The *amip-piForcing* $\tilde{\alpha}_E$
 742 is particularly small around 1940 because the pattern and global mean have opposite
 743 effects on the trend in R , while it is particularly large around 1990 because their effects
 744 have the same sign. We conjecture that these findings could be linked if volcanic forcing
 745 has a pattern effect that gives large $\tilde{\alpha}$ in both *amip-piForcing* and *historical*, but with
 746 different time-dependence.

747 For information about the effect of volcanoes, we turn to *historicalNat*. There is
 748 greater similarity in time-dependence of $\tilde{\alpha}_E$ since 1930 between *historicalNat* and *amip-*
 749 *piForcing* than between *historical* and *amip-piForcing* (Figure 5c). Although all three
 750 have smaller $\tilde{\alpha}_E$ in the first half of the twentieth century (higher EffCS), the minimum
 751 has a similar magnitude and date (around 1940) in *amip-piForcing* and *historicalNat*,
 752 while *historical* is increasing by then, having reached its minimum earlier and at a
 753 larger value. Moreover, $\tilde{\alpha}_E$ is minimum (highest EffCS) in recent decades in *historical*,
 754 but maximum (lowest EffCS) and similar in *amip-piForcing* and *historicalNat*. During
 755 this period in the latter two experiments $\tilde{\alpha}_E$ is close to $2.3 \text{ W m}^{-2} \text{ K}^{-1}$ (magenta cross
 756 in Figure 5c, EffCS 1.6 K), which is the value calculated from observational estimates
 757 for 1985–2011 for T (HadCRUT4 blended land and sea surface temperature, Morice
 758 et al 2012) and N (ERBE and CERES satellite measurements of TOA radiative flux,
 759 Allan et al 2014) with the AR5 F .

760 Despite the similarity of the timeseries of $\tilde{\alpha}_E(t)$ in *amip-piForcing* and *historical-*
 761 *Nat*, their $R(t)$ timeseries look quite different (Figure 8a,b). In *historicalNat*, imme-
 762 diately after each major volcanic eruption, there is a large negative spike in R , which
 763 then returns to zero over ~ 10 years. The same structure is apparent in R in the *histor-*
 764 *ical* experiment, where it is superimposed on the positive trend due to global warming.
 765 The episodic covariation of volcanically forced T and R gives the large $\tilde{\alpha}_E \simeq 2.5$
 766 $\text{W m}^{-2} \text{ K}^{-1}$ of *historicalNat* for the period since 1975 (green in Figure 6b).

767 In the same period, while *amip-piForcing* has a similar $\tilde{\alpha}_E$ (blue line), it does not
 768 show unusually large variations in R at the times of eruptions (Figure 8a); on the con-
 769 trary, it has larger excursions at other times, presumably due to unforced variability.
 770 The same difference of character can be seen when comparing T from the CMIP5 *his-*
 771 *torical* experiment with the observational estimate (Figure 2). Rapid cooling following
 772 major eruptions is clear in CMIP5, but not in observations.

773 The forced response in R to volcanoes is obvious in the *historicalNat* multimodel
 774 mean (green line in Figure 8b), because the unforced variability has been intentionally
 775 suppressed by taking the mean. The negative spikes in R should also be present in *amip-*
 776 *piForcing* if the CMIP5 simulated forced response is realistic. Because *amip-piForcing*
 777 is driven by the observed record of SST, which is a single realisation of history rather
 778 than a mean, we expect that unforced variability will be larger than in the *historicalNat*
 779 multimodel mean, and could cancel out a volcanic spike by chance.

780 However, it seems unlikely that *all* the historical major eruptions would have been
 781 obscured in this way. The *historicalNat* multimodel mean $R(t)$ falls below -0.3 W m^{-2}
 782 following the eruptions of Krakatau, Agung, Santa Maria and Pinatubo (green line in
 783 Figure 8b). The same is true for all four of these eruptions in the majority of the 31
 784 individual *historicalNat* integrations (Table 2), where we count $R < -0.3 \text{ W m}^{-2}$ in the
 785 year of the eruption or in either of the following two years as a volcanic signal. There
 786 is no *historicalNat* integration in which fewer than two of these four eruptions produce
 787 such a signal, but *none* of them does in *amip-piForcing* R (blue line in Figure 8a).

788 An alternative possibility is that unforced variability in R is larger in the real world
 789 than in CMIP5 AOGCMs, and dwarfs all variations of the size of the forced volcanic

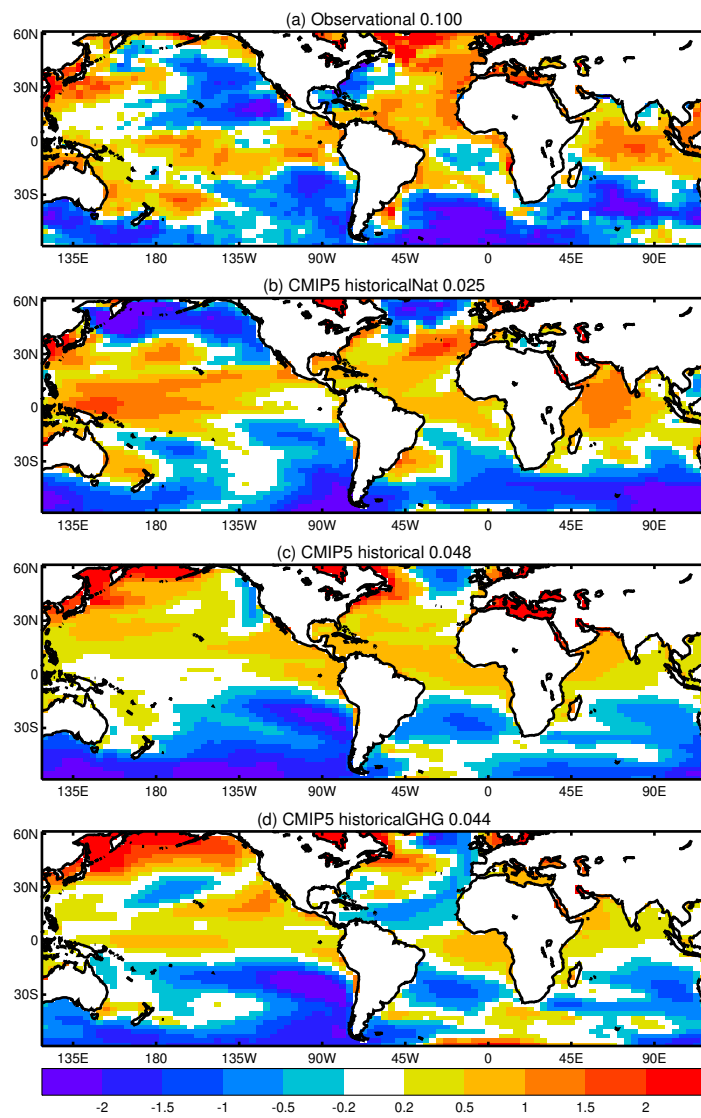


Fig. 9 Normalised pattern (K K^{-1} , see text for derivation) of SST change 1975–2004 within 65°S – 65°N in the (a) AMIP II observational dataset, (b,c,d) multimodel mean of CMIP5 *historicalNat*, *historical* and *historicalGHG* experiments, respectively. The numbers shown in the titles of the panels are the spatial standard deviations of SST variation explained by regression (K , see text for derivation).

790 signal. Indeed, the magnitude and duration of accelerated trade winds and sea level
 791 trends in the Pacific during this period also exceed their occurrence in *piControl* exper-
 792 iments (England et al 2014; Bilbao et al 2015). Such large unforced variability would
 793 dominate the T - R relationship throughout the historical period. Neither anthropogenic
 794 nor natural forced signals would be discernible; instead $\tilde{\alpha}_E$ would be fairly steady, like
 795 in the individual *historical* integrations ($\tilde{\alpha}_i$ of MPI-ESM1.1 and $\tilde{\alpha}_I$ of CMIP5 in Fig-
 796 ure 5a, Section 5.1). This is quite unlike what we see in *amip-piForcing* (Figures 5c
 797 and 6b).

798 Therefore we suggest that CMIP5 AOGCMs are not realistic in their response to
 799 volcanic forcing. In the real world, represented by *amip-piForcing*, volcanic forcing does
 800 not cause a large rapid cooling of T , as it does in CMIP5. Instead, volcanic forcing
 801 “sucks” heat from the ocean beneath. The system reacts as though it had a large heat
 802 capacity, so that $T \simeq 0 \Rightarrow R \simeq 0 \Rightarrow N \simeq F < 0$, yielding a negative spike in N . We
 803 suggest that, in both the real world and CMIP5, the volcanically forced SST pattern
 804 gives a large α , but that it lasts for longer in the real world. Following the eruption,
 805 the pattern of SST change causes $R > 0$ for a decade or two, perhaps through some
 806 persistent response to the subsurface cooling (discussed in Section 7). Consequently the
 807 volcanic episodes since 1960 are not distinct in the real world, but form a continuous
 808 period.

809 In support of this suggestion, we note that the normalised patterns of SST varia-
 810 tion during 1975–2004 in *historicalNat* and observations have some similarities (Fig-
 811 ure 9a,b), especially regarding features in the North and low-latitude Pacific. On the
 812 other hand, the normalised patterns of the *historical* and *historicalGHG* experiments
 813 (Figure 9c,d) resemble each other in these regions. For these “normalised patterns”, we
 814 exclude areas poleward of 65° , where observational SST data is sparse and the com-
 815 parison with model data is complicated by the treatment of sea-ice. We regress local
 816 annual-mean SST over the 30 years against its area-mean within 65°S – 65°N , to obtain
 817 a pattern in K K^{-1} with unit mean. Note that any correlated variation of local SST
 818 and global mean will contribute to this pattern, both trends and variability. Finally we
 819 subtract unity uniformly, and divide by the spatial standard deviation. The result is a
 820 field with zero mean and unit standard deviation.

821 The observed and *historicalNat* patterns could be consistent with a low EffCS
 822 because the warming in the west Pacific in these patterns leads to large upper tropo-
 823 spheric warming, giving large negative lapse-rate feedback, and increased stability in
 824 the low-cloud regions, giving small or negative cloud feedback (Zhou et al 2016; Ceppi
 825 and Gregory 2017; Andrews and Webb 2018). Further GCM experiments or analyses
 826 are needed to establish how the differences in the observed and CMIP5 SST patterns
 827 lead to their various values of α .

828 Although the pattern of SST change in *historicalNat* is somewhat similar to ob-
 829 servations, it is much less pronounced, as shown by smaller magnitude of SST vari-
 830 ation explained by regression in *historicalNat* (0.025 K) compared with observations
 831 (0.100 K). (This number is the spatial standard deviation of the field obtained from
 832 multiplying the pattern in K K^{-1} from the regression, before normalisation, by the
 833 temporal standard deviation of T . This field quantifies the local temporal variation of
 834 SST due to the global-mean temporal variation.) The comparison suggests that the
 835 AOGCMs respond with a realistic pattern to volcanic forcing, but too weakly. Conse-
 836 quently the stronger SST variation due to greenhouse-gas forcing (0.044 K) is able to
 837 overwhelm the volcanic pattern during 1975–2004 in the CMIP5 *historical* experiment,
 838 making $\tilde{\alpha}_E$ similar to *historicalGHG* (Figure 5c). In the real world, on the other hand,

839 the volcanic response is persistent and dominant, and accounts for the low EffCS of
840 the AMIP period.

841 7 Summary, discussion and conclusions

842 7.1 How accurately can CO₂ EffCS be estimated from historical EffCS?

843 Many calculations have been published of the effective climate sensitivity (EffCS),
844 *i.e.* the equilibrium warming of global-mean surface air temperature for doubled CO₂,
845 as estimated from non-equilibrium states or radiative forcings other than $2 \times \text{CO}_2$.
846 Some calculations use observed climate change during the historical period, others
847 use GCM simulations of climate change with idealised elevated CO₂ concentration.
848 For convenience, we refer to these two kinds of estimate as “historical” and “CO₂”.
849 Both historical EffCS and CO₂ EffCS have a wide spread (Knutti et al 2017). We have
850 quantified several reasons for the differences among these estimates, in order to address
851 the question which supplies the title of this work.

852 First, the estimate of the climate feedback parameter α using ordinary least-square
853 regression (OLS) of the global-mean top-of-atmosphere radiative response against the
854 global-mean surface temperature change from a *single* realisation of historical change
855 (such as the real world) is both uncertain and biased towards low values by the presence
856 of unforced variability. The bias causes $\text{EffCS} \propto 1/\alpha$ to be overestimated, in the mul-
857 timodel mean by about 10% for regression of the entire historical period, and 20% for
858 30-year periods. It is unimportant in scenarios of strong forcing, such as *abrupt4xCO2*,
859 but cannot be neglected when considering historical variations.

860 Second, evaluating historical EffCS is hampered by the systematic uncertainty in
861 the forcing F , which in CMIP5 AOGCMs gives a $\pm 45\%$ uncertainty in historical Eff-
862 CS. The present phase of the Coupled Model Intercomparison Project contains new
863 experiments which should greatly reduce the spread in all the model forcings, but an
864 accurate estimate of real-world historical EffCS from the global-mean energy balance
865 depends on reduction of the uncertainty in real-world historical F , assessed as about
866 $\pm 30\%$ by the AR5.

867 Third, α varies substantially on multidecadal timescales, according both to AOGCM
868 *historical* experiments, which simulate climate change in response to forcing agents, and
869 to AGCM *amip-piForcing* experiments, in which observed historical sea surface tem-
870 perature is prescribed. This means that historical EffCS depends on the period from
871 which it is evaluated. The *historical* and *amip-piForcing* experiments indicate that for
872 most of the historical period the EffCS was smaller (α larger) than CO₂ EffCS, by up
873 to a factor of ~ 2 at some times. This bias is in the opposite direction to and therefore
874 not explained by bias in the OLS slope.

875 The time-variation of α in the *historical* experiments can mainly be explained by the
876 varying relative importance of greenhouse gas and volcanic aerosol forcing, provided
877 that the EffCS for volcanic aerosol forcing is smaller than for CO₂ forcing (*i.e.* its
878 efficacy is less than unity), so that historical EffCS falls below CO₂ EffCS during
879 volcanically affected periods. As a result, the EffCS from regression of the *historical*
880 multimodel mean for the entire historical period is about 5% lower than CO₂ EffCS.

881 The time-variation of α in the *amip-piForcing* experiments is due to the evolving
882 patterns of SST, and synchronised in all the AGCMs because of their common boundary
883 conditions. The EffCS from regression of the *amip-piForcing* multimodel mean for the

entire historical period is about 30% less than CO₂ EffCS, a much greater bias than in the *historical* multimodel mean.

AOGCM *historical* and AGCM *amip-piForcing* experiments agree that the EffCS was relatively high in the period around 1940, when there were no large volcanic eruptions, and both greenhouse-gas and anthropogenic aerosol forcings were increasing in magnitude. The EffCS for this period in *amip-piForcing* has a range of 2.1–4.6 K, and is highly correlated with AOGCM CO₂ EffCS across models. The agreement increases confidence in this range as an estimate of CO₂ EffCS.

Since 1960, there have been three large volcanic eruptions. During this period, EffCS falls to its lowest values in *amip-piForcing*, of around 1.6 K, in agreement with our observational estimate for the 27 years around 1998, and consistent with low EffCS for volcanic forcing. On the other hand, EffCS increases since 1960 in the *historical* experiment, converges with the *historicalGHG* EffCS, and is correlated across AOGCMs with the CO₂ EffCS. We further discuss the disagreement between *historical* and *amip-piForcing* in Section 7.2.

Nearly 30 years have now passed since the eruption of Pinatubo, similar to the interval between the eruption of Katmai and 1940, so we might expect that the EffCS has returned to its CO₂ value, although another decade of observations may be required to demonstrate it clearly. Because greenhouse-gas forcing is increasing more rapidly now than in the early 20th century, the OLS bias in α will be less important. We therefore consider that the EffCS of the first 30 years of the present century may give the most accurate energy-balance historical estimate of CO₂ EffCS, especially if the uncertainty in F can be reduced, unless another explosive volcanic eruption occurs.

7.2 SST and EffCS since 1975

We have carried out AGCM experiments to show that the observed pattern of SST change during 1975–2004 (the final 30 years of the CMIP5 *historical* experiments) induces heat loss from the climate system, producing the historically low EffCS that is simulated in *amip-piForcing*, and suppressing the greenhouse warming. In some respects this pattern (Figure 9a,b) resembles the Interdecadal Pacific Oscillation, which has been associated with the reduced rate or hiatus of global warming during the early twenty-first century, through the influence of accelerated Pacific trade winds on ocean heat uptake (England et al 2014; Meehl et al 2016; Oka and Watanabe 2017; Xie and Kosaka 2017).

The observed pattern of SST change during 1975–2004 has some similarities to the pattern that results during the same period from volcanic forcing in the AOGCM *historicalNat* experiment, including for instance the contrast between strong warming in the western Pacific and cooling or weak warming in the east, consistent with feedbacks giving a low EffCS (Zhou et al 2016; Ceppi and Gregory 2017; Andrews and Webb 2018). However, the amplitude is much weaker in *historicalNat* than in observations. Therefore in the *historical* experiment the volcanic pattern is overwhelmed by the greenhouse-gas pattern as the latter forcing increases, whereas in the real world the similar but stronger pattern has continued to dominate. This explains why α for recent decades is larger (EffCS smaller) when estimated from observations or AGCM *amip-piForcing* experiments than from AOGCM *historical* experiments.

There are several possible causes of the observed SST pattern, apart from volcanic forcing. It could be forced by anthropogenic aerosol (Smith et al 2016), which is not

distinguished in our analysis of the time-dependence of the EffCS. It could be due to an internal mode of Pacific interannual variability that is stimulated by the response to or recovery from volcanic forcing (Emile-Geay et al 2008; Maher et al 2015; Khodri et al 2017; Hua et al 2018; Eddebbar et al 2019), or it could be due entirely to unforced variability.

Whatever the cause, it is striking that α in *amip-piForcing*, associated with this pattern, reaches such a large value, given that it is derived from the single realisation of observed climate history. This contrasts with the AOGCMs, in which we found α evaluated from a single integration to be biased low by the presence of unforced variability (Appendix C), and comparably large values are attained only in the multimodel mean. We speculate that there are coupled atmosphere-ocean feedbacks which reinforce this SST pattern in the real world but are lacking in models (McGregor et al 2014; Raedel et al 2016; Yuan et al 2018; Liu et al 2018; McGregor et al 2018).

The divergence of *historical* and *amip-piForcing* α indicates either that the AOGCM forced response is unrealistic, or that unforced variability has recently taken the EffCS outside the range it shows in *piControl* experiments. Either explanation implies a deficiency in AOGCMs, and calls for further investigation.

7.3 Prospects for estimating the climate response to CO₂

There are powerful reasons for wanting to evaluate the CO₂ EffCS from existing historical data, rather than waiting until we have accumulated enough further years of greenhouse-gas-forced climate change to enable an accurate energy-budget estimate. For the period since the 1980s, an estimate of EffCS can already be made from the observed energy budget (subject to systematic uncertainty in F), but this may be an underestimate of the CO₂ EffCS, due to pattern effects (Sections 7.1 and 7.2). To avoid this problem, GCMs have been used to obtain relationships between historical and CO₂-forced EffCS that may be used to correct observationally derived estimates of the EffCS (Armour 2017; Andrews et al 2018). However, such methods suffer from systematic uncertainty owing to their dependence on the SST patterns being correctly represented by GCMs.

In order to make better use of the observed data and to refine or constrain AOGCM projections of the future, we need to study the interactions of the forcings, climate feedbacks and ocean heat uptake with the spatiotemporal patterns of SST change. Although such an analysis is more difficult than appealing to the historical global energy balance, it is necessary because the assumption that a single constant global climate feedback parameter can describe the responses to all forcings on all timescales is clearly inadequate.

Appendices

A The step model

The step model (Good et al 2011; Hansen et al 2011; Good et al 2013; Gregory et al 2016) is based on the assumption that the climate responses $X_i(t)$ in the quantities of interest (T and N) to separate forcings $F_i(t)$ combine linearly to give $X(t) = \sum_i X_i(t)$ in response to the forcings applied together as $F(t) = \sum_i F_i(t)$. By assuming further that the response to any step-change in forcing depends only on the size of the step and not the nature of the

973 forcing agent, we can estimate the response to historical time-dependent net forcing $F(t)$
 974 due to all agents by treating it as the sum of a set of discrete steps in forcing, such that
 975 $F(t) = \sum_{j=1}^t [F(j) - F(j-1)]$ where j are successive instants of time (we use a timestep of
 976 one year) and $F(0) = 0$. The response of an AOGCM at time t to the forcing increment which
 977 occurred at time $j < t$ is estimated as $X_{4\times}(t-j+1)[F(j) - F(j-1)]/F_{4\times}$, where $X_{4\times}$
 978 is the AOGCM’s time-dependent response to the step-change forcing $F_{4\times}$ in the *abrupt4xCO2*
 979 experiment, since time t is timestep $t-j+1$ since the forcing increment $[F(j) - F(j-1)]$
 980 occurred. Hence, adding up the response to all previous increments,

$$X(t) = \sum_{j=1}^t X_{4\times}(t-j+1) \frac{F(j) - F(j-1)}{F_{4\times}}.$$

981 Note that the step-model makes no assumption about the value or time-variation of α , except
 982 that it is the same for all magnitudes and kinds of forcing.

983 B Choice of independent variable for regression

984 Ordinary least-squares (OLS) linear regression assumes that all variations in the independent
 985 variable x cause proportionate variations in the dependent variable y . If there is “noise” in y ,
 986 meaning fluctuations that are linearly uncorrelated with the “signal”, which is a function of
 987 x , the OLS estimate of the slope dy/dx is imprecise, with a standard error that increases with
 988 the amplitude of the noise (Appendix D.2), but it is unbiased, meaning that expectation value
 989 of the estimate equals the true value. On the other hand, if our data for x contain some noise
 990 which does not cause variations in y *i.e.* the “true” independent x on which y depends is not
 991 precisely known (possible sources of such noise are considered in Section 4), the OLS estimate
 992 of the slope is biased. It is expected to be smaller than the true value, and the bias grows with
 993 the amplitude of the noise (Appendix D.3).

994 Therefore if one of the variables contains noise which is not correlated with the other
 995 variable, the former should be chosen as dependent and the latter as independent, in order to
 996 obtain an unbiased estimate of the slope. This is the natural choice for a situation where the
 997 independent variable is chosen precisely by the experimenter, and the dependent variable is
 998 measured with some uncertainty. In our application, N and T are physically both dependent
 999 on the prescribed F , so it is not obvious which of $R = F - N$ or T we should select as the
 1000 independent variable.

1001 Because random error is small in the MPI-ESM1.1 *historical* ensemble mean, we expect
 1002 the bias in the estimated slope to be small, regardless of whether T or R is chosen as the inde-
 1003 pendent variable. The correlation between T and R is less than unity, so the slopes for the two
 1004 choices are not quite equal (Appendix D.4), but they are close, namely $1.36 \pm 0.04 \text{ W m}^{-2} \text{ K}^{-1}$
 1005 for regression of ensemble-mean R against ensemble-mean T , denoted by $\bar{\alpha}_e$ (Table 1, solid line
 1006 in Figure 4), and $1.54 \pm 0.05 \text{ W m}^{-2} \text{ K}^{-1}$ for T against R (dashed line), where the standard
 1007 error is inferred from the residual of the fit. Therefore the *historical* slope for the ensemble
 1008 mean is $\bar{\alpha}_e = 1.4\text{--}1.5 \text{ W m}^{-2} \text{ K}^{-1}$, assuming the underlying physical relationship is truly linear.

1009 The mean of the ensemble of slopes obtained by regression of R against T in the individual
 1010 integrations is $\bar{\alpha}_i = 1.38 \pm 0.01 \text{ W m}^{-2} \text{ K}^{-1}$ (mean and standard error), not shown in Figure 4
 1011 because it is statistically indistinguishable from $\bar{\alpha}_e$. However, the mean of the slopes from
 1012 individual members when we regress T against R is quite different (dotted line in Figure 4,
 1013 slope of $2.08 \pm 0.01 \text{ W m}^{-2} \text{ K}^{-1}$), and looks like a poor fit to the ensemble-mean data. This
 1014 bias is the expected outcome of OLS regression of y against x when x contains noise which is
 1015 uncorrelated with y (Appendix D.3). If there is uncorrelated noise in R , linear regression of T
 1016 against R gives an estimate of dT/dR which is biased low, and hence its reciprocal $\bar{\alpha} = dR/dT$
 1017 is biased high.

1018 To minimise the bias, we prefer to choose T as the independent variable for OLS regression
 1019 (Appendix D.4), assuming that the noise in R is not correlated with T . Certainly, there appears
 1020 to be *more* noise in R than in T (Figure 3), consistent with physical understanding that T
 1021 is related to the time-integral of N , (although a similar bias in the slope could be caused by
 1022 correlated noise in T and R , Appendix D.6). The results from the MPI-ESM1.1 are consistent
 1023 with assuming that T contains *no* noise, but this may not hold for other AOGCMs.

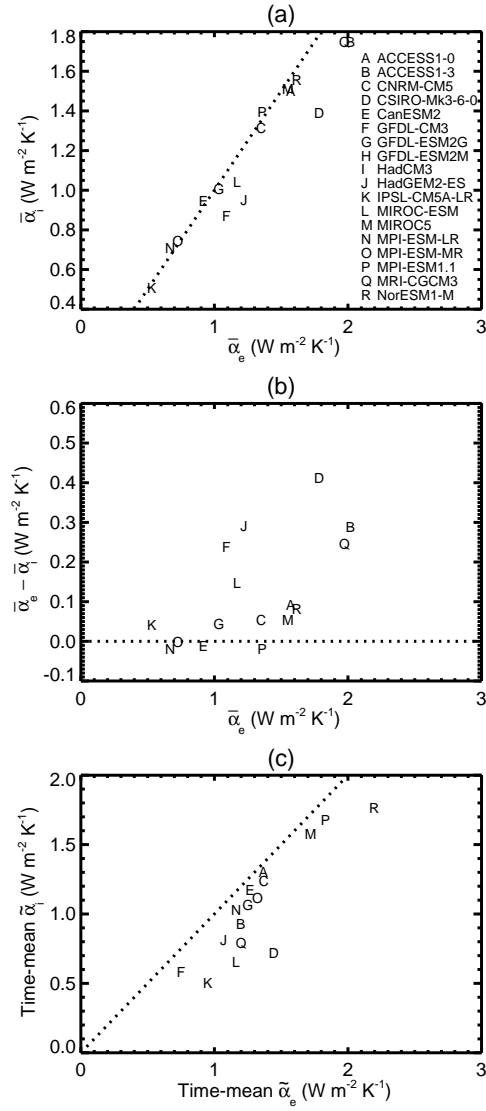


Fig. 10 Relationships in CMIP5 AOGCM *historical* experiments between α evaluated from the ensemble-mean $R(t)$ and $T(t)$, and the ensemble-mean of α evaluated from $R(t)$ and $T(t)$ in individual integrations, (a,b) between $\bar{\alpha}_i$ and $\bar{\alpha}_e$, (c) between time-mean $\tilde{\alpha}_i$ and time-mean $\tilde{\alpha}_e$ (see Table 1 for notation). Only those AOGCMs which have more than one ensemble member are included (see Table 2). We use our AR5' estimate for *historical* $F(t)$ for all AOGCMs except HadGEM2-ES and MPI-ESM1.1 (models J and P), for which we use $F(t)$ diagnosed in these models individually (compared in Figure 1). The dotted line in (b) is zero on the vertical axis; all models lie very near or above this line, indicating that $\bar{\alpha}_e - \bar{\alpha}_i \geq 0$. The dotted line in (a,c) is 1:1; all models lie very near or to the right of this line in (a), indicating that $\bar{\alpha}_e \geq \bar{\alpha}_i$ (consistent with b), and in (c), indicating that time-mean $\tilde{\alpha}_e \geq$ time-mean $\tilde{\alpha}_i$.

1024 C Error in estimating climate feedback from a single ensemble member

1025 Using the HadGEM2 *historical* F (Section 3.1), we carry out the calculations of Appendix B
 1026 for the HadGEM2-ES *historical* ensemble, which comprises only five members, a typical size for
 1027 CMIP5 submissions. We obtain $\bar{\alpha}_i = 0.94 \pm 0.10 \text{ W m}^{-2} \text{ K}^{-1}$ and $\bar{\alpha}_e = 1.22 \pm 0.14 \text{ W m}^{-2} \text{ K}^{-1}$,
 1028 thus $\bar{\alpha}_e > \bar{\alpha}_i$, unlike MPI-ESM1.1, in which we found above that $\bar{\alpha}_e \simeq \bar{\alpha}_i$. The correlation
 1029 coefficient between ensemble-mean R and T is 0.59, weaker than for MPI-ESM1.1 due to the
 1030 smaller ensemble size and consequently greater noise in the ensemble mean.

1031 For the same calculations with the *historical* experiments of other CMIP5 AOGCMs we use
 1032 our AR5' estimate for $F(t)$ (Section 3.3), because F has not been diagnosed in these models.
 1033 Since F is model-dependent, it may differ from the AR5' estimate, so $\bar{\alpha}$ from the regression
 1034 could be inaccurate; that would be a systematic error that affects all the ensemble members
 1035 of each model equally, rather than a statistical uncertainty affecting them randomly. Within
 1036 each model ensemble, noise produces a spread of $\bar{\alpha}$. The geometrical multimodel mean of the
 1037 ensemble standard deviation of $\bar{\alpha}$ is $0.11 \text{ W m}^{-2} \text{ K}^{-1}$, $\sim 10\%$ of the multimodel-mean $\bar{\alpha}_e$.

1038 Across AOGCMs, the correlation coefficient of $\bar{\alpha}_i$ and $\bar{\alpha}_e$ is very high (0.96, Figure 10a)
 1039 but $\bar{\alpha}_e > \bar{\alpha}_i$ (Figure 10b), as for HadGEM2-ES, except in the MPI and CanESM2 AOGCMs,
 1040 in which $\bar{\alpha}_e \simeq \bar{\alpha}_i$. This is consistent with the bias of OLS regression whereby the slope is
 1041 underestimated when there is noise in T that is not correlated with R (Appendix B); because
 1042 the noise is larger in individual integrations than in the ensemble mean, $\bar{\alpha}_i$ is underestimated
 1043 more severely than $\bar{\alpha}_e$. Furthermore, the bias tends to be greater for larger $\bar{\alpha}_e$ (Figure 10b,
 1044 correlation 0.61), consistent with the same explanation (Appendix D.3). The multimodel-mean
 1045 underestimate of $\bar{\alpha}_i$ with respect to $\bar{\alpha}_e$ is 10%.

1046 As mentioned in Section 1, estimates of α using observed N can be made only from the
 1047 more recent ~ 30 years, since interannual variation of N is not well enough known at earlier
 1048 times. To evaluate the effect of the OLS bias on α estimated from a 30-year period, denoted by
 1049 $\tilde{\alpha}$ (Table 1), with each AOGCM we regress R against T for 30-year periods starting in every
 1050 year (*i.e.* they overlap) in every integration, obtaining a timeseries $\tilde{\alpha}(t)$ for each integration
 1051 (following Gregory and Andrews 2016). From these we calculate the ensemble-mean timeseries,
 1052 denoted by $\bar{\tilde{\alpha}}(t)$, and its historical time-mean. The time-mean is the expectation value of $\tilde{\alpha}$ for
 1053 a randomly chosen 30-year period of a single integration. The geometrical multimodel mean
 1054 of the ensemble standard deviation of $\tilde{\alpha}$, pooled over years in each model, is $0.42 \text{ W m}^{-2} \text{ K}^{-1}$,
 1055 30% of the multimodel-mean time-mean $\bar{\tilde{\alpha}}_e$. Similarly, from the ensemble-mean R and T of
 1056 each model we compute the $\tilde{\alpha}_e(t)$ for 30-year periods and its historical time-mean.

1057 Across models, the correlation coefficient of the time-means of $\tilde{\alpha}_i$ and $\tilde{\alpha}_e$ is high (0.88),
 1058 but time-mean $\tilde{\alpha}_e$ is greater in all cases (Figure 10c), consistent with a greater bias of OLS
 1059 regression for a randomly chosen 30-year period of a single integration than of the ensemble
 1060 mean, just as for $\bar{\alpha}_i$ and $\bar{\alpha}_e$, but the effect is more pronounced because the noise is more
 1061 important for a shorter period. The multimodel-mean underestimate of $\tilde{\alpha}_i$ with respect to $\tilde{\alpha}_e$
 1062 is 20%. Since the CMIP5 ensembles are fairly small, it is likely that $\tilde{\alpha}_e$ is also biased, and the
 1063 underestimate of the true value therefore greater.

1064 D Statistical issues in regression

1065 In this appendix, we consider various statistical issues related to the estimation of α as the
 1066 slope of the regression of R against T . These issues apply more generally than to those specific
 1067 variables. The general problem is to estimate the slope m in the linear relationship $y(t) =$
 1068 $m x(t)$, where x and y are timeseries of length n with values at times $t = \tau_1, \tau_2, \dots, \tau_n$, given
 1069 the data \hat{x}_i and \hat{y}_i , which may differ from x and y because of random noise. (To simplify
 1070 the formulae we have chosen the origin so that the means of x and y are zero.) In the model
 1071 world, we may have an ensemble of integrations $i = 1, \dots, N$, with the same x and y in all but
 1072 different noise in each. For ensemble member i , we obtain an estimate $\hat{m}_i = \text{cov}(\hat{x}_i, \hat{y}_i) / \text{var}(\hat{x}_i)$
 1073 of $m = dy/dx$ by ordinary least-squares linear regression (OLS) of $\hat{y}_i(t)$ against $\hat{x}_i(t)$. The OLS
 1074 estimate minimises the root-mean-square (RMS) of the residuals of the $y_i(t)$ from the fitted
 1075 line in the y -direction. By doing so it maximises the likelihood that the residuals are consistent
 1076 with independent identically distributed random noise $\epsilon_i(t)$ in y .

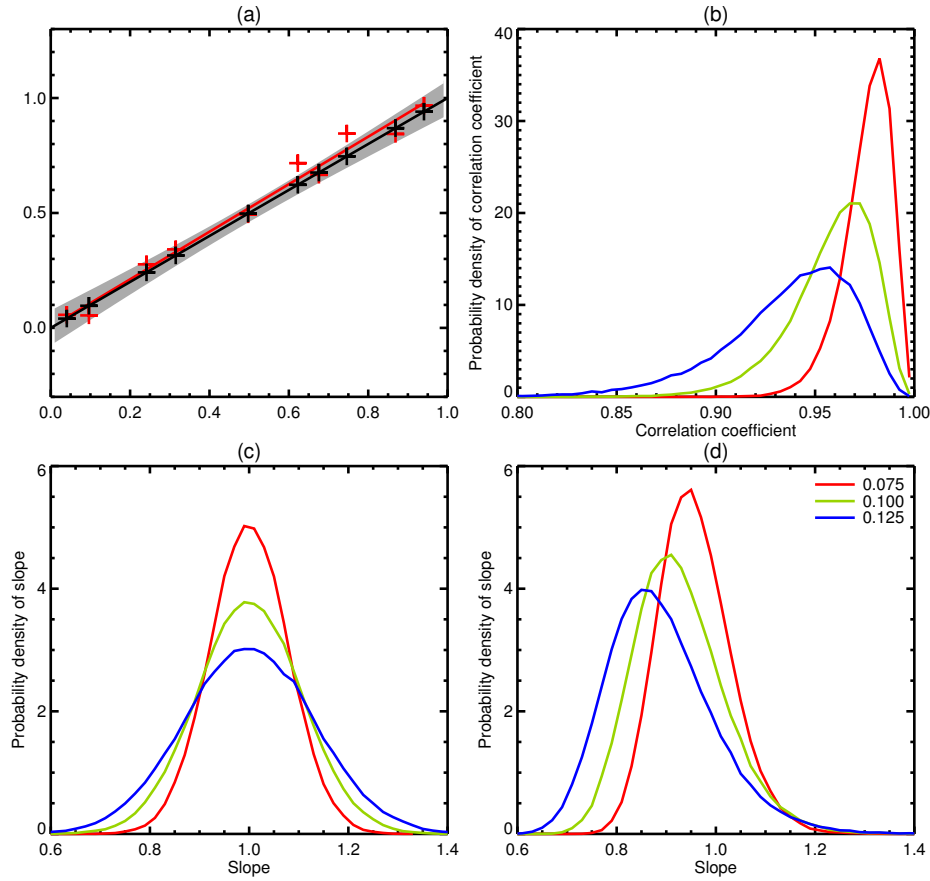


Fig. 11 Illustration of the effect of random noise on ordinary least squares regression. We take the $x(t)$ shown in black in (a), with a slope of unity so that $y = x$, generate many sets of $\hat{x}_i(t)$ and $\hat{y}_i(t)$ by adding noise either to y or x , and calculate the distribution of estimated slopes. (a) Red shows an example with noise in y of standard deviation 0.075 and its regression line, grey envelope is the 5–95% range of regression lines; (b) distribution of correlation coefficients between $\hat{x}_i(t)$ and $\hat{y}_i(t)$ with noise in either x or y ; (c,d) distribution of slopes of regression lines when there is noise in y or x respectively; (b,c,d) each show results for noise with three different standard deviations, as indicated by the key in (d).

1077 D.1 The difference method is a special case of regression

1078 In the special case of $n = 2$, whatever the noise may be, a straight line can be drawn exactly
 1079 through the two points $\hat{x} = x_0 \pm \frac{1}{2}\Delta x$ and $\hat{y} = y_0 \pm \frac{1}{2}\Delta y$, leaving zero residual. Denoting
 1080 a mean by $M(\cdot)$, we obtain $M(\hat{x}) = x_0$, $M(\hat{y}) = y_0$, $\text{var}(\hat{x}) = M(\hat{x}^2) - (M(\hat{x}))^2 = (\frac{1}{2}\Delta x)^2$,
 1081 $\text{cov}(\hat{x}, \hat{y}) = M(\hat{x}\hat{y}) - M(\hat{x})M(\hat{y}) = \frac{1}{4}\Delta x \Delta y$. Hence for this case the OLS formula gives $\hat{m} =$
 1082 $\text{var}(\hat{x})/\text{cov}(\hat{x}, \hat{y}) = \Delta y/\Delta x$, the slope of the line passing through the points. Therefore \hat{m}
 1083 estimated as the slope between the endpoints in \hat{x} is a special case of OLS, using a minimal
 1084 amount of data, and the results derived in this appendix, that \hat{m} is uncertain and may be
 1085 biased on account of noise in x and y , apply to the difference method (Equation 2) just as
 1086 they do to regression (Equation 3).

1087 D.2 No bias in \hat{m} due to uncorrelated noise in y

1088 The rationale for the use of OLS is that the independent variable \hat{x}_i is perfectly known
1089 but the dependent variable \hat{y}_i is noisy,

$$\hat{x}_i(t) = x(t) \quad \hat{y}_i(t) = y(t) + \epsilon_i(t) = mx(t) + \epsilon_i(t). \quad (4)$$

1090 With these assumptions, $\text{var}(\hat{x}) = \text{var}(x)$, and

$$\text{cov}(\hat{x}, \hat{y}) = \text{cov}(x, mx + \epsilon) = M(x(mx + \epsilon)) - M(x)M(mx + \epsilon) = m \text{var}(x) + M(x\epsilon)$$

1091 since $M(x) = 0$. Therefore the OLS slope

$$\hat{m} = \frac{\text{cov}(\hat{x}, \hat{y})}{\text{var}(\hat{x})} = m + \frac{M(x\epsilon)}{\text{var}(x)}$$

1092 is an imprecise estimate of m . However, the expectation value $E(\hat{m}) = m$, because $E(M(x\epsilon)) =$
1093 0 if there is *no correlation* between x and ϵ ; we call the noise “uncorrelated” to indicate that is
1094 not correlated with x or y . Thus, the OLS estimate of the slope is not biased by the presence
1095 of uncorrelated noise in y .

1096 To illustrate this, we choose a set of $n = 10$ random numbers $x(t)$ in the interval 0–1,
1097 and take $m = 1 \Rightarrow y = x$ (x , y and $y = x$ are shown in black in Figure 11a). We generate
1098 $N = 10^5$ instances of $\hat{y}_i(t)$ from $y(t)$ by adding independent normally distributed $\epsilon_i(t)$ with
1099 standard deviation of 0.075. The correlation coefficients of x with \hat{y}_i have a positively skewed
1100 distribution (red in Figure 11b). We regress each $\hat{y}_i(t)$ against $x(t)$ to obtain \hat{m}_i (an example
1101 \hat{y}_i and its regression line are shown in red in Figure 11a). The distribution of \hat{m} is normal,
1102 its mean is $m = 1$ and its standard deviation 0.079 (red in Figure 11c). If we increase the
1103 amplitude of noise to 0.100 and 0.125, \hat{m} remains unbiased but becomes less precise (standard
1104 deviation of 0.105 for green and 0.131 for blue in Figure 11c), and the correlation is degraded
1105 gradually (Figure 11b).

1106 Although x was chosen randomly, there is no uncorrelated noise in x in this example,
1107 because $\hat{x}_i = x_i$. For example, we might have

$$\hat{x}_i(t) = x_i(t) = x(t) + \xi_i(t) \quad \hat{y}_i(t) = y_i + \epsilon_i(t) = mx_i(t) + \epsilon_i(t) = mx(t) + m\xi_i(t) + \epsilon_i(t), \quad (5)$$

1108 where $x(t)$ is the response to external forcing and the same in all ensemble members, while
1109 $\xi_i(t)$ is unforced variability that is different in each member. Although ξ might be called “noise
1110 in x ”, it is *perfectly correlated* with noise $m\xi$ in y . If all variations x' in \hat{x} , however they are
1111 caused, produce corresponding variations mx' in \hat{y} , \hat{m} will be an unbiased estimate of m . If x
1112 and y are T and R , this is the case which Proistosescu et al (2018) call “ocean-forced”.

1113 D.3 Bias in \hat{m} due to uncorrelated noise in x

1114 If y is not noisy but x contains uncorrelated noise $\delta_i(t)$ in ensemble member i , we have

$$\hat{x}_i(t) = x(t) + \delta_i(t) \quad \hat{y}_i(t) = y(t) = mx(t), \quad (6)$$

1115 which differs from Equation (5) because the variations δ in \hat{x} do not produce proportionate
1116 variations $m\delta$ in \hat{y} . In this situation

$$\begin{aligned} \text{cov}(\hat{x}, \hat{y}) &= \text{cov}(x + \delta, mx) = M((x + \delta)mx) - M(x + \delta)M(mx) \\ &= m \text{var}(x) + mM(x\delta), \end{aligned}$$

1117 and

$$\text{var}(\hat{x}) = M((x + \delta)^2) - (M(x + \delta))^2 = \text{var}(x) + \text{var}(\delta) + 2M(x\delta). \quad (7)$$

1118 Similiar to Section D.2, $E(M(x\delta)) = 0$ for uncorrelated noise, giving

$$\hat{m} = \frac{\text{cov}(\hat{x}, \hat{y})}{\text{var}(\hat{x})} \simeq \frac{m}{1 + \text{var}(\delta)/\text{var}(x)} < m$$

1119 *i.e.* the estimate of the slope is not only imprecise, but also biased low if there is uncorrelated
 1120 noise in x . (We have written this as an approximation because the expectation value of a ratio
 1121 does not exactly equal the ratio of expectation values.) The slope is underestimated, through
 1122 the appearance of $\text{var}(\delta)$ in the denominator, because OLS assumes that all variations in \hat{x}
 1123 cause variations in \hat{y} . The larger the ratio of noise to signal $\text{var}(\delta)/\text{var}(x)$, the greater the bias.
 1124 This bias has been called “regression dilution” (Frost and Thompson 2000).

1125 We illustrate this case with the same $x(t)$ and $y(t)$ as the previous case, but this time we
 1126 take $\hat{y}(t) = y(t)$ and generate N instances of $\hat{x}_i(t)$ from $x(t)$ by adding independent normally
 1127 distributed $\delta_i(t)$. The distribution of \hat{m}_i from regressing $y(t)$ against $\hat{x}_i(t)$ is negatively skewed
 1128 and biased low (median 0.95, 5–95% range 0.85–1.09, red in Figure 11d). For larger noise, the
 1129 spread and the bias both increase (median 0.92 for green and 0.88 for blue in Figure 11d). The
 1130 distribution of correlation coefficients in the three cases are the same as for noise in y , because
 1131 the formula is symmetrical in x and y .

1132 In our application we are estimating $m = \alpha$ from $R = y$ and $T = x$. The expected
 1133 magnitude of the bias in $\hat{\alpha}$ is therefore

$$E(\hat{\alpha}) - \alpha = \frac{-\text{var}(\delta)}{\text{var}(T) + \text{var}(\delta)} \alpha.$$

1134 If $\text{var}(T)$ and $\text{var}(\delta)$ are independent of α , this formula predicts that the expected bias in
 1135 $\hat{\alpha}$ will increase in proportion to α . In our set of model simulations of the past, $\text{var}(T)$ is
 1136 not independent of α , because we expect that a model with a larger α (smaller EffCS) will
 1137 produce a smaller historical T increase. This makes $\text{var}(T)$ smaller, $1/(\text{var}(T) + \text{var}(\delta))$ larger,
 1138 and strengthens the dependence of the expected negative bias $E(\hat{\alpha}) - \alpha$ upon α .

1139 D.4 Correct choice of independent variable

1140 If y is independent and perfectly known while x is dependent and noisy, we should instead
 1141 minimise the RMS deviations of the x from the fitted line in the x -direction, obtaining from
 1142 ensemble member i an estimate $\hat{m}_i^\dagger = \text{cov}(\hat{x}_i, \hat{y}_i)/\text{var}(\hat{y}_i)$ of the slope dx/dy . The product
 1143 $\hat{m}_i^\dagger \hat{m}_i = (\text{cov}(\hat{x}_i, \hat{y}_i))^2/(\text{var}(\hat{x}_i)\text{var}(\hat{y}_i)) = r_i^2$, where r_i is the (product-moment) correlation
 1144 coefficient between \hat{x}_i and \hat{y}_i . Thus the lines fitted in the two ways have equal slopes $\hat{m}_i = 1/\hat{m}_i^\dagger$
 1145 if and only if \hat{x}_i and \hat{y}_i are perfectly correlated or anticorrelated ($r_i = \pm 1$).

1146 In the usual situation of imperfect correlation, the choice of independent variable therefore
 1147 makes a difference to the OLS estimate of the slope. This is because of the bias caused by
 1148 noise in the independent variable (Section D.3). If one of the variables is noisy and the other
 1149 is not, we must treat the noisy variable as the dependent one to get an unbiased estimate of
 1150 the slope.

1151 D.5 Uncorrelated noise in both x and y

1152 If there is independent noise in both x and y , we cannot get an unbiased estimate of m using
 1153 OLS. This case can be treated with “orthogonal” or “total least-squares” regression, in
 1154 which the RMS deviation of the points from the line is minimised in a direction orthogonal
 1155 to the line, but that requires a prior estimate of the relative size of δ and ϵ , which we do not
 1156 have. Other methods, called “error in variables”, have been developed for this case (*e.g.* Cahill
 1157 et al 2015).

1158 D.6 Correlated noise in x and y

1159 Another situation to consider is that of *correlated* noise in x and y . Suppose that

$$\hat{x}_i(t) = x(t) + \xi_i(t) \quad \hat{y}_i(t) = mx(t) + \mu\xi_i(t) + \epsilon_i(t), \quad (8)$$

1160 where μ is a constant and ξ_i is noise that is different in each ensemble member. Because
 1161 ξ_i affects both \hat{x}_i and \hat{y}_i , the noise $\hat{x}_i(t) - x_i(t) = \xi_i(t)$ in x and the noise $\hat{y}_i(t) - y_i(t) =$
 1162 $\mu\xi_i(t) + \epsilon_i(t)$ in y have a non-zero correlation coefficient $\mu \text{var}(\xi) / \sqrt{\mu^2 \text{var}(\xi) + \text{var}(\epsilon)}$. Now by
 1163 following the method of Appendix D.3 we obtain

$$E(\hat{m}) = E\left(\frac{\text{cov}(\hat{x}, \hat{y})}{\text{var}(\hat{x})}\right) \simeq \frac{m \text{var}(x) + \mu \text{var}(\xi)}{\text{var}(x) + \text{var}(\xi)} = m \frac{1 + (\mu/m)(\text{var}(\xi)/\text{var}(x))}{1 + (\text{var}(\xi)/\text{var}(x))},$$

1164 assuming x and ξ are uncorrelated.

1165 This case is more general than, and encompasses, all of those previously considered. If
 1166 $\text{var}(\xi) \ll \text{var}(x)$, the noise in x is negligible, and we recover $E(\hat{m}) = m$. If $\mu = m$, $y_i(t) =$
 1167 $m(x_i(t) + \xi_i(t))$, as in Equation (5), in which case we have shown that $E(\hat{m}) = m$ still (Ap-
 1168 pendix D.2). If $\mu = 0$, the noise in x and y is decorrelated, and $E(\hat{m}) = m/(1 + \text{var}(\xi)/\text{var}(x)) <$
 1169 m (as in Appendix D.3). The general formula with $\mu \neq 0$ applies to two relevant physical sit-
 1170 uations in which T is x , R is y and m is the climate feedback parameter for forced climate
 1171 change on multidecadal timescales.

1172 Firstly, suppose there is unforced variability that arises spontaneously in N and causes
 1173 correlated variability T' in T . This is the case which Proistosescu et al (2018) call “radiatively
 1174 forced”, and we describe it qualitatively in Section 4. We can illustrate the effect with a simple
 1175 model. Suppose that the spontaneous random variability $\Phi(t)$ in $N(t)$ has a stepwise
 1176 behaviour, such that $\Phi(t) = \Phi_j$ for $\tau_j \leq t < \tau_{j+1}$, with a step-change in N of $\Phi_j - \Phi_{j-1}$ at
 1177 $t = \tau_j$. According to the step model (Appendix A), the response of T' to Φ is

$$T'(t) = \sum_{k=-\infty}^j \Theta(t - \tau_k)(\Phi_k - \Phi_{k-1}) = \Theta(t - \tau_j)\Phi_j + \sum_{k=-\infty}^j \Phi_{k-1}(\Theta(t - \tau_{k-1}) - \Theta(t - \tau_k))$$

1178 for $\tau_j \leq t < \tau_{j+1}$, where $\Theta(t)$ is the response of T per unit step-change in forcing at $t = 0$. This
 1179 T' response will add a further perturbation $\alpha T'$ to N , assuming the same climate feedback
 1180 parameter α applies to both forced and unforced variations. If $T_F(t)$ is the response of T to
 1181 external forcing $F(t)$, we have $T = T_F + T'$, $N = F - \alpha T_F + \Phi_j - \alpha T'$ and $R = F - N =$
 1182 $\alpha T_F - \Phi_j + \alpha T'$. We can rewrite this as

$$T(t) = T_F(t) + H(t) + \Theta(t - \tau_j)\Phi_j \quad R(t) = \alpha(T_F(t) + H(t)) + \Phi_j(\alpha\Theta(t - \tau_j) - 1)$$

1183 with

$$H(t) \equiv \sum_{k=-\infty}^j \Phi_{k-1}(\Theta(t - \tau_{k-1}) - \Theta(t - \tau_k)).$$

1184 This has the form of Equation (8) for correlated noise, with $x = T_F + H$, $\xi = \Theta(t - \tau_j)\Phi_j$,
 1185 $y = R$, $\mu = (\alpha\Theta(t - \tau_j) - 1)/\Theta(t - \tau_j) = \alpha - 1/\Theta(t - \tau_j)$ and $m = \alpha$, where H is the response
 1186 of T to Φ earlier than τ_j .

1187 Physically, the correlation arises because the noise in T is the response to Φ_j , while the
 1188 noise in R is the sum of Φ_j itself and the response in N to Φ_j . Since the responses to Φ_j in both
 1189 N and T are proportional to Φ_j , the noise in R and T is correlated. From $\mu = m - 1/\Theta(t - \tau_j)$
 1190 we obtain $\mu - m = -1/\Theta(t - \tau_j) < 0$ because for climate stability we must have $\Theta(t) > 0$. Hence
 1191 $\mu < m \Rightarrow E(\hat{m}) < m$. The climate feedback parameter will inevitably be underestimated if the
 1192 correlation is due to spontaneous fluctuations in N . The effect is therefore similar to regression
 1193 dilution (Appendix D.3) but it is not formally the same.

1194 The correlation is present because both Φ and T have non-zero timescales of change. A zero
 1195 timescale of response in T means it changes instantly when the energy balance is perturbed,
 1196 keeping the system always in equilibrium with $\alpha T = F + \Phi$. This requires $\Theta(t) = 1/\alpha$ for all
 1197 $t > 0$, and hence $\mu = 0$, so the correlation vanishes. With stepwise variation, Φ has persistence
 1198 with a non-zero timescale. This can be removed by replacing its step-changes at times τ_j
 1199 with δ -function spikes. In that case $\Phi = 0$ between these times, and Φ_j does not appear in
 1200 $R = \alpha(T_F + T')$. This is the situation of perfectly correlated noise described by Equation (5),
 1201 with $\xi = T'$, effectively the same as no noise, because signal and noise cannot be distinguished.

1202 Secondly, ξ could represent unforced variability that arises spontaneously in T on inter-
 1203 annual timescales, causing an immediate radiative response in R that may have a climate
 1204 feedback parameter $\mu \neq m$. The estimate of m obtained by regression of R against T will be
 1205 biased in the direction of μ by unforced variability. The larger $\text{var}(\xi)/\text{var}(x)$, the greater the

1206 bias. The ratio will be large if unforced variability is large, or if the record is short and hence
 1207 shows little forced change. Unlike the previous cases, the bias in \hat{m} could be in either direction;
 1208 when $\mu \leq m$, $E(\hat{m}) \leq m$.

1209 **Acknowledgements** We are grateful to Luis Kornblueh for proposing the 100-member MPI-
 1210 ESM1.1 *historical* ensemble, to the coauthors of Andrews et al (2018) for the use of their
 1211 *amip-piForcing* data, to Andy Dessler, Rob Colman, Jean-Louis Dufresne and other col-
 1212 leagues at CFMIP meetings for useful discussions, to Andy Dessler for useful comments on the
 1213 manuscript, and to Michel Crucifix and two anonymous reviewers for their thorough, thought-
 1214 ful and constructive comments. This project has received funding from the European Research
 1215 Council (ERC) under the European Union’s Horizon 2020 research and innovation programme
 1216 (grant agreement 786427, project “Couplet”). Work at the Met Office was supported by the
 1217 Joint UK BEIS/Defra Met Office Hadley Centre Climate Programme (GA01101). Paulo Ceppi
 1218 was supported by an Imperial College Research Fellowship. We acknowledge the World Climate
 1219 Research Programme’s Working Group on Coupled Modelling, which is responsible for CMIP,
 1220 and we thank the climate modeling groups (listed in Table 2 of this paper) for producing and
 1221 making available their model output.

1222 References

- 1223 Abraham JP, Baringer M, Bindoff NL, Boyer T, Cheng LJ, Church JA, Conroy JL, Domingues
 1224 CM, Fasullo JT, Gilson J, Goni G, Good SA, Gorman JM, Gouretski V, Ishii M, Johnson
 1225 GC, Kizu S, Lyman JM, Macdonald AM, Minkowycz WJ, Moffitt SE, Palmer MD, Piola
 1226 AR, Resegetti F, Schuckmann K, Trenberth KE, Velicogna I, Willis JK (2013) A review
 1227 of global ocean temperature observations: Implications for ocean heat content estimates
 1228 and climate change. *Rev Geophys* 51(3):450–483, DOI 10.1002/rog.20022
- 1229 Allan RP, Liu C, Loeb NG, Palmer MD, Roberts M, Smith D, Vidale PL (2014) Changes
 1230 in global net radiative imbalance 1985–2012. *Geophys Res Lett* 41:5588–5597, DOI
 1231 10.1002/2014GL060962
- 1232 Andrews T (2014) Using an AGCM to diagnose historical effective radiative forcing and mech-
 1233 anisms of recent decadal climate change. *J Climate* 27:1193–1209, DOI 10.1175/JCLI-D-
 1234 13-00336.1
- 1235 Andrews T, Webb MJ (2018) The dependence of global cloud and lapse rate feedbacks on the
 1236 spatial structure of tropical Pacific warming. *J Climate* 31:641–654, DOI 10.1175/JCLI-
 1237 D-17-0087.1
- 1238 Andrews T, Gregory JM, Webb MJ, Taylor KE (2012) Forcing, feedbacks and climate sensitiv-
 1239 ity in CMIP5 coupled atmosphere-ocean climate models. *Geophys Res Lett* 39(7):L09,712,
 1240 DOI 10.1029/2012GL051607
- 1241 Andrews T, Gregory JM, Webb MJ (2015) The dependence of radiative forcing and feedback
 1242 on evolving patterns of surface temperature change in climate models. *J Climate* 28:1630–
 1243 1648, DOI 10.1175/JCLI-D-14-00545.1
- 1244 Andrews T, Betts RA, Booth BBB, Jones CD, Jones GS (2017) Effective radiative forcing
 1245 from historical land use change. *Clim Dyn* 48:3489–3505, DOI 10.1007/s00382-016-3280-7
- 1246 Andrews T, Gregory JM, Paynter D, Silvers LG, Zhou C, Mauritsen T, Webb MJ, Armour KC,
 1247 Forster PM, Titchner H (2018) Accounting for changing temperature patterns increases his-
 1248 torical estimates of climate sensitivity. *Geophys Res Lett* 45, DOI 10.1029/2018GL078887
- 1249 Armour KC (2017) Energy budget constraints on climate sensitivity in light of inconstant
 1250 climate feedbacks. *Nature Climate Change* pp 1–8, DOI 10.1038/nclimate3278
- 1251 Armour KC, Bitz CM, Roe GH (2013) Time-varying climate sensitivity from regional feed-
 1252 backs. *J Climate* 26:4518–4534, DOI 10.1175/JCLI-D-12-00544.1
- 1253 Barnes EA, Barnes RJ (2015) Estimating linear trends: simple linear regression versus epoch
 1254 differences. *J Climate* 28:9969–9976, DOI 10.1175/JCLI-D-15-0032.1
- 1255 Bengtsson L, Schwartz SE (2013) Determination of a lower bound on Earths climate sensitivity.
 1256 *Tellus B* 65:21,533, DOI 10.3402/tellusb.v65i0.21533
- 1257 Bilbao RAF, Gregory JM, Bouttes N (2015) Analysis of the regional pattern of sea level
 1258 change due to ocean dynamics and density changes for 1993–2099 in observations and
 1259 CMIP5 AOGCMs. *Clim Dyn* 45():2647–2666, DOI 10.1007/s00382-015-2499-z

- 1260 Bloch-Johnson J, Pierrehumbert RT, Abbot D (2015) Feedback temperature depen-
1261 dence and equilibrium climate sensitivity. *Geophys Res Lett* 42():4973–4980, DOI
1262 10.1002/2015GL064240
- 1263 Cahill N, Kemp AC, Horton BP, Parnell AC (2015) Modeling sea-level change using errors-
1264 in-variables integrated Gaussian processes. *Ann Appl Stat* 9:547–571, DOI 10.1214/15-
1265 AOAS824
- 1266 Ceppi P, Gregory JM (2017) Relationship of tropospheric stability to climate sensitivity and
1267 earth’s observed radiation budget. *Proc Natl Acad Sci USA* 114():13,126–13,131, DOI
1268 10.1073/pnas.1714308114
- 1269 Ceppi P, Gregory JM (in press) A refined model for the earth’s global energy balance. *Clim*
1270 *Dyn* DOI 10.1007/s00382-019-04825-x
- 1271 Chung ES, Soden BJ (2015) An assessment of direct radiative forcing, radiative adjustments,
1272 and radiative feedbacks in coupled oceanatmosphere models. *J Climate* 28(10):4152–4170,
1273 DOI 10.1175/JCLI-D-14-00436.1
- 1274 Colman R, Power SB (2018) What can decadal variability tell us about climate feedbacks and
1275 sensitivity? *Clim Dyn* 51:3815–3828, DOI 10.1007/s00382-018-4113-7
- 1276 Dessler AE (2013) Observations of climate feedbacks over 2000–10 and comparisons to climate
1277 models. *J Climate* 26:333–342, DOI 10.1175/JCLI-D-11-00640.1
- 1278 Dessler AE, Mauritsen T, Stevens B (2018) The influence of internal variability on Earth’s
1279 energy balance framework and implications for estimating climate sensitivity. *Atmos Chem*
1280 *Phys* 18:5147–5155, DOI 10.5194/acp-18-5147-2018
- 1281 Eddebbar YA, Rodgers KB, Long MC, Subramanian AC, Xie SP, Keeling RF (2019) El
1282 Niñolike physical and biogeochemical ocean response to tropical eruptions. *J Climate*
1283 32(9):2627–2649, DOI 10.1175/JCLI-D-18-0458.1
- 1284 Emile-Geay J, Seager R, Cane MA, Cook ER, Haug GH (2008) Volcanoes and ENSO over the
1285 past millennium. *J Climate* 21:3134–3148, DOI 10.1175/2007JCLI1884.1
- 1286 England MH, McGregor S, Spence P, Meehl GA, Timmermann A, Cai W, Gupta AS,
1287 McPhaden MJ, Purich A, Santoso A (2014) Recent intensification of wind-driven circula-
1288 tion in the Pacific and the ongoing warming hiatus. *Nature Climate Change* 4(3):222–227,
1289 DOI 10.1038/nclimate2106
- 1290 Flato G, Marotzke J, Abiodun B, Braconnot P, Chou SC, Collins W, Cox P, Driouech F,
1291 Emori S, Eyring V, Forest C, Gleckler P, Guilyardi E, Jakob C, Kattsov V, Reason C,
1292 Rummukainen M (2013) Evaluation of climate models. In: Stocker TF, Qin D, Plattner
1293 GK, Tignor M, Allen SK, Boschung J, Nauels A, Xia Y, Bex V, Midgley PM (eds) *Climate*
1294 *Change 2013: The Physical Science Basis. Contribution of Working Group I to the*
1295 *Fifth Assessment Report of the Intergovernmental Panel on Climate Change*, Cambridge
1296 University Press, pp 741–866, DOI 10.1017/CBO9781107415324.020
- 1297 Forster PM (2016) Inference of climate sensitivity from analysis of the Earth’s energy budget.
1298 *Annu Rev Earth Planet Sci* 44, DOI 10.1146/annurev-earth-060614-105156
- 1299 Forster PM, Andrews T, Good P, Gregory JM, Jackson LS, Zelinka M (2013) Evaluating ad-
1300 justed forcing and model spread for historical and future scenarios in the CMIP5 generation
1301 of climate models. *J Geophys Res* 118:1–12, DOI 10.1002/jgrd.50174
- 1302 Forster PMDF, Gregory JM (2006) The climate sensitivity and its components diagnosed from
1303 Earth radiation budget data. *J Climate* 19():39–52, DOI 10.1175/JCLI3611.1
- 1304 Frost C, Thompson SG (2000) Correcting for regression dilution bias: comparison of meth-
1305 ods for a single predictor variable. *J R Statist Soc A* 163:173–189, DOI 10.1111/1467-
1306 985X.00164
- 1307 Gates WL, Boyle JS, Covey C, Dease CG, Doutriaux CM, Drach RS, Fiorino M, Gleckler
1308 PJ, Hnilo JJ, Marlais SM, Phillips TJ, Potter GL, Santer BD, Sperber KR, Taylor KE,
1309 Williams DN (1999) An overview of the results of the Atmospheric Model Intercomparison
1310 Project (AMIP I). *Bull Am Meteorol Soc* 80(1):29–55
- 1311 Giorgetta MA, Jungclaus J, Reick CH, Legutke S, Bader J, Boettinger M, Brovkin V, Crueger
1312 T, Esch M, Fieg K, Glushak K, Gayler V, Haak H, Hollweg HD, Ilyina T, Kinne S,
1313 Kornblueh L, Matei D, Mauritsen T, Mikolajewicz U, Mueller W, Notz D, Pithan F,
1314 Raddatz T, Rast S, Redler R, Roeckner E, Schmidt H, Schnur R, Segsneider J, Six KD,
1315 Stockhause M, Timmreck C, Wegner J, Widmann H, Wieners KH, Claussen M, Marotzke
1316 J, Stevens B (2013) Climate and carbon cycle changes from 1850 to 2100 in MPI-ESM
1317 simulations for the Coupled Model Intercomparison Project phase 5. *J Adv Model Earth*
1318 *Syst* 5:572–597, DOI 10.1002/jame.20038

- 1319 Good P, Gregory JM, Lowe JA (2011) A step-response simple climate model to reconstruct and
1320 interpret AOGCM projections. *Geophys Res Lett* 38:L01,703, DOI 10.1029/2010GL045208
- 1321 Good P, Ingram W, Lambert FH, Lowe JA, Gregory JM, Webb MJ, Ringer MA, Wu P (2012) A
1322 step-response approach for predicting and understanding non-linear precipitation changes.
1323 *Clim Dyn* 39:2789–2803, DOI 10.1007/s00382-012-1571-1
- 1324 Good P, Gregory JM, Lowe JA, Andrews T (2013) Abrupt CO₂ experiments as tools for
1325 predicting and understanding CMIP5 representative concentration pathway projections.
1326 *Clim Dyn* 40():1041–1053, DOI 10.1007/s00382-012-1410-4
- 1327 Gordon C, Cooper C, Senior CA, Banks H, Gregory JM, Johns TC, Mitchell JFB, Wood
1328 RA (2000) The simulation of SST, sea ice extents and ocean heat transports in a version
1329 of the Hadley Centre coupled model without flux adjustments. *Clim Dyn* 16():147–168,
1330 DOI 10.1007/s003820050010
- 1331 Gregory JM, Andrews T (2016) Variation in climate sensitivity and feedback parameters during
1332 the historical period. *Geophys Res Lett* 43():3911–3920, DOI 10.1002/2016GL068406
- 1333 Gregory JM, Forster PM (2008) Transient climate response estimated from radiative
1334 forcing and observed temperature change. *J Geophys Res* 113:D23,105, DOI
1335 10.1029/2008JD010405
- 1336 Gregory JM, Stouffer RJ, Raper SCB, Stott PA, Rayner NA (2002) An observationally
1337 based estimate of the climate sensitivity. *J Climate* 15():3117–3121, DOI 10.1175/1520-
1338 0442(2002)015<3117:AOBEOT>2.0.CO;2
- 1339 Gregory JM, Ingram WJ, Palmer MA, Jones GS, Stott PA, Thorpe RB, Lowe JA, Johns TC,
1340 Williams KD (2004) A new method for diagnosing radiative forcing and climate sensitivity.
1341 *Geophys Res Lett* 31:L03,205, DOI 10.1029/2003gl018747
- 1342 Gregory JM, Andrews T, Good P (2015) The inconstancy of the transient climate response
1343 parameter under increasing CO₂. *Philos Trans R Soc London* 373():20140,417, DOI
1344 10.1098/rsta.2014.0417
- 1345 Gregory JM, Andrews T, Good P, Mauritsen T, Forster PM (2016) Small global-mean cooling
1346 due to volcanic radiative forcing. *Clim Dyn* 47():3979–3991, DOI 10.1007/s00382-016-3055-
1347 1
- 1348 Grose MR, Gregory J, Colman R, Andrews T (2018) What climate sensitivity index is most
1349 useful for projections? *Geophys Res Lett* 45():1559–1566, DOI 10.1002/2017GL075742
- 1350 Hansen J, Sato M, Nazarenko L, Ruedy R, Lacis A, Koch D, Tegen I, Hall T, Shindell D, Santer
1351 B, Stone P, Novakov T, Thomason L, Wang R, Wang Y, Jacob D, Hollandsworth-Frith
1352 S, Bishop L, Logan J, Thompson A, Stolarski R, Lean J, Willson R, Levitus S, Antonov
1353 J, Rayner N, Parker D, Christy J (2002) Climate forcings in Goddard Institute for Space
1354 Studies SI2000 simulations. *J Geophys Res* 107, DOI 10.1029/2001JD001143
- 1355 Hansen J, Sato M, Rudy R, Nazarenko L, Lacis A, Schmidt GA, Russell G, Aleinov I, Bauer
1356 M, Bauer S, Bell N, Cairns B, Canuto V, Chandler M, Cheng Y, Del Genio A, Faluvegi G,
1357 Fleming E, Friend A, Hall T, Jackman C, Kelley M, Kiang N, Koch D, Lean J, Lerner J,
1358 Lo K, Menon S, Miller R, Romanou A, Shindell D, Stone P, Sun S, Tausnev N, Thresher
1359 D, Wielicki B, Wong T, Yao M, Zhang S (2005) Efficacy of climate forcings. *J Geophys*
1360 *Res* 110:D18,104, DOI 10.1029/2005JD005776
- 1361 Hansen J, Sato M, Kharecha P, Von Schuckmann K (2011) Earth’s energy imbalance and
1362 implications. *Atmos Chem Phys* 11:13,421–13,449, DOI 10.5194/acp-11-13421-2011
- 1363 Hartmann DL, Klein Tank AMG, Rusticucci M, Alexander LV, Brönnimann S, Charabi Y,
1364 Dentener FJ, Dlugokencky EJ, Easterling DR, Kaplan A, Soden BJ, Thorne PW, Wild M,
1365 Zhai PM (2013) Observations: Atmosphere and surface. In: Stocker TF, Qin D, Plattner
1366 GK, Tignor M, Allen SK, Boschung J, Nauels A, Xia Y, Bex V, Midgley PM (eds) *Climate*
1367 *Change 2013: The Physical Science Basis. Contribution of Working Group I to the*
1368 *Fifth Assessment Report of the Intergovernmental Panel on Climate Change*, Cambridge
1369 University Press, DOI 10.1017/CBO9781107415324.008
- 1370 Haugstad AD, Armour KC, Battisti DS, Rose BEJ (2017) Relative roles of surface temperature
1371 and climate forcing patterns in the inconstancy of radiative feedbacks. *Geophys Res Lett*
1372 44, DOI 10.1002/2017GL074372
- 1373 Held IM, Winton M, Takahashi K, Delworth T, Zeng F, Vallis GK (2010) Probing the fast
1374 and slow components of global warming by returning abruptly to preindustrial forcing. *J*
1375 *Climate* 23:2418–2427, DOI 10.1175/2009JCLI3466.1
- 1376 Hua W, Dai A, Qin M (2018) Contributions of internal variability and external forcing to the
1377 recent Pacific decadal variations. *Geophys Res Lett* 45, DOI 10.1029/2018GL079033

- 1378 Hurrell JW, Hack JJ, Shea D, Caron JM, Rosinski J (2008) A new sea surface temperature and
1379 sea ice boundary dataset for the Community Atmosphere Model. *J Climate* 21:5145–5153,
1380 DOI 10.1175/2008JCLI2292.1
- 1381 Jones GS, Stott PA, Christidis N (2013) Attribution of observed historical near surface temper-
1382 ature variations to anthropogenic and natural causes using cmip5 simulations. *J Geophys*
1383 *Res* 18(10):4001–4024, DOI 10.1002/jgrd.50239
- 1384 Jonko AK, Shell KM, Sanderson BM, Danabasoglu G (2012) Climate feedbacks in CCSM3
1385 under changing CO₂ forcing. Part II: Variation of climate feedbacks and sensitivity with
1386 forcing. *J Climate* 26:2784–2795, DOI 10.1175/JCLI-D-12-00479.1
- 1387 Kamae Y, Chadwick R, Ackerley D, Ringer M, Ogur T (2019) Seasonally variant low cloud
1388 adjustment over cool oceans. *Clim Dyn* 52:5801–5817, DOI 10.1007/s00382-018-4478-7
- 1389 Khodri M, Izumo T, Vialard J, Janicot S, Cassou C, Lengaigne M, Mignot J, Gastineau
1390 G, Guilyardi E, Lebas N, Robock A, McPhaden MJ (2017) Tropical explosive volcanic
1391 eruptions can trigger El Niño by cooling tropical Africa. *Nat Commun* 8:778, DOI
1392 10.1038/s41467-017-00755-6
- 1393 Knutti R, Rugenstein MAA, Hegerl GC (2017) Beyond equilibrium climate sensitivity. *Nat*
1394 *Geosci* 10:727–736, DOI 10.1038/NNGEO3017
- 1395 Larson EJJ, Portmann RW (2016) A temporal kernel method to compute effective radiative
1396 forcing in CMIP5 transient simulations. *J Climate* 29():1497–1509, DOI 10.1175/JCLI-D-
1397 15-0577.1
- 1398 Liu F, Lu J, Garuba O, Leung LR, Luo Y, Wan X (2018) Sensitivity of surface temperature to
1399 oceanic forcing via q -flux Green’s function experiments. Part I: Linear response function.
1400 *J Climate* 31:3625–3641, DOI 10.1175/JCLI-D-17-0462.1
- 1401 Lutsko NJ, Takahashi K (2018) What can the internal variability of cmip5 models tell us about
1402 their climate sensitivity? *J Climate* 31:5051–5069, DOI 10.1175/JCLI-D-17-0736.1
- 1403 Maher N, McGregor S, England MH, Sen Gupta A (2015) Effects of volcanism on tropical
1404 variability. *Geophys Res Lett* 42:6024–6033, DOI 10.1002/2015GL064751
- 1405 Marvel K, Schmidt GA, Miller RL, Nazarenko LS (2016) Implications for climate sensitiv-
1406 ity from the response to individual forcings. *Nature Climate Change* 6:386–389, DOI
1407 10.1038/NCLIMATE2888
- 1408 Marvel K, Pincus R, Schmidt GA, Miller RL (2018) Internal variability and disequilibrium
1409 confound estimates of climate sensitivity from observations. *Geophys Res Lett* 45:1595–
1410 1601, DOI 10.1002/2017GL076468
- 1411 McGregor S, Timmermann A, Stuecker MF, England MH, Merrifield M, Jin FF, Chikamoto Y
1412 (2014) Recent Walker circulation strengthening and Pacific cooling amplified by Atlantic
1413 warming. *Nature Climate Change* 4(10):888–892, DOI 10.1038/nclimate2330
- 1414 McGregor S, Stuecker MF, Kajtar JB, England MH, Collins M (2018) Model tropical atlantic
1415 biases underpin diminished pacific decadal variability. *Nature Climate Change* 8:493–498,
1416 DOI 10.1038/s41558-018-0163-4
- 1417 Meehl GA, Hu A, Santer BD, Xie SP (2016) Contribution of the Interdecadal Pacific Oscillation
1418 to twentieth-century global surface temperature trends. *Nature Climate Change* 6:1005–
1419 1008, DOI 10.1038/NCLIMATE3107
- 1420 Meraner K, Mauritsen T, Voigt A (2013) Robust increase in equilibrium climate sensitivity
1421 under global warming. *Geophys Res Lett* 40:5944–5948, DOI 10.1002/2013GL058118
- 1422 Mitchell JFB, Manabe S, Meleshko V, Tokioka T (1990) Equilibrium climate change—and
1423 its implications for the future. In: Houghton JT, Jenkins GJ, Ephraums JJ (eds) *Climate*
1424 *change: the IPCC scientific assessment*, Cambridge University Press, chap 5, pp 131–172
- 1425 Morice CP, Kennedy JJ, Rayner NA, Jones PD (2012) Quantifying uncertainties in global
1426 and regional temperature change using an ensemble of observational estimates: The Had-
1427 CRUT4 data set. *J Geophys Res* 117():D08,101, DOI doi:10.1029/2011JD017187
- 1428 Myhre G, Shindell D, Bréon FM, Collins W, Fuglestedt J, Huang J, Koch D, Lamarque JF,
1429 Lee D, Mendoza B, Nakajima T, Robock A, Stephens G, Takemura T, Zhang H (2013)
1430 Anthropogenic and natural radiative forcing. In: Stocker TF, Qin D, Plattner GK, Tignor
1431 M, Allen SK, Boschung J, Nauels A, Xia Y, Bex V, Midgley PM (eds) *Climate Change*
1432 *2013: The Physical Science Basis. Contribution of Working Group I to the Fifth Assessment*
1433 *Report of the Intergovernmental Panel on Climate Change*, Cambridge University Press,
1434 pp 659–740, DOI 10.1017/CBO9781107415324.018
- 1435 Oka A, Watanabe M (2017) The post-2002 global surface warming slowdown caused by the
1436 subtropical Southern Ocean heating acceleration. *Geophys Res Lett* 44:3319–3327, DOI
1437 10.1002/2016GL072184

- 1438 Otto A, Otto FEL, Boucher O, Church J, Hegerl G, Forster PM, Gillett NP, Gregory J,
1439 Johnson GC, Knutti R, Lewis N, Lohmann U, Marotzke J, Myhre G, Shindell D, Stevens
1440 B, Allen MR (2013) Energy budget constraints on climate response. *Nature Geosci* 6:415–
1441 416, DOI 10.1038/ngeo1836
- 1442 Palmer MD (2017) Reconciling estimates of ocean heating and Earth’s radiation budget. *Cur-*
1443 *rent Climate Change Reports* 3:78–86, DOI 10.1007/s40641-016-0053-7
- 1444 Paynter D, Frölicher TL (2015) Sensitivity of radiative forcing, ocean heat uptake, and cli-
1445 mate feedback to changes in anthropogenic greenhouse gases and aerosols. *J Geophys Res*
1446 120:98379854, DOI 10.1002/2015JD023364
- 1447 Pincus R, Forster PM, Stevens B (2016) The Radiative Forcing Model Intercomparison Project
1448 (RFMIP): Experimental protocol for CMIP6. *Geosci Model Devel* 9:3447–3460, DOI
1449 10.5194/gmd-9-3447-2016
- 1450 Proistosescu C, Donohoe A, Armour KC, Roe GH, Stuecker MF, Bitz CM (2018) Radiative
1451 feedbacks from stochastic variability in surface temperature and radiative imbalance. *Geo-*
1452 *phys Res Lett* 45:5082–5094, DOI 10.1029/2018GL077678
- 1453 Raedel G, Mauritsen T, Stevens B, Dommenges D, Matei D, Bellomo K, Clement A (2016)
1454 Amplification of El Niño by cloud longwave coupling to atmospheric circulation. *Nat Geosci*
1455 9:106–111, DOI 10.1038/NCEO2630
- 1456 Reichler T, Kim J (2008) How well do coupled models simulate today’s climate? *Bull Am*
1457 *Meteorol Soc* 89(3):303–311, DOI 10.1175/BAMS-89-3-303
- 1458 Ringer MA, Andrews T, Webb MJ (2014) Global-mean radiative feedbacks and forcing in
1459 atmosphere-only and coupled atmosphere-ocean climate change experiments. *Geophys Res*
1460 *Lett* 41:4035–4042, DOI 10.1002/2014GL060347
- 1461 Roemmich D, Church J, Gilson J, Monselesan D, Sutton P, Wijffels S (2015) Unabated plan-
1462 etary warming and its ocean structure since 2006. *Nature Climate Change* 5:240–245,
1463 DOI 10.1038/NCLIMATE2513
- 1464 Sherwood S, Bony S, Boucher O, Bretherton C, Forster P, Gregory J, Stevens B (2015) Ad-
1465 justments in the forcing-feedback framework for understanding climate change. *Bull Am*
1466 *Meteorol Soc* 96():217–228, DOI 10.1175/BAMS-D-13-00167.1
- 1467 Shindell D (2014) Inhomogeneous forcing and transient climate sensitivity. *Nature Climate*
1468 *Change* 4:274–277, DOI 10.1038/NCLIMATE2136
- 1469 Shine KP, Cook J, Highwood EJ, Joshi MM (2003) An alternative to radiative forcing for esti-
1470 mating the relative importance of climate change mechanisms. *Geophys Res Lett* 30:2047,
1471 DOI 10.1029/2003GL018141
- 1472 Silvers LG, Paynter D, Zhao M (2018) The diversity of cloud responses to twentieth century
1473 sea surface temperatures. *Geophys Res Lett* 45:391–400, DOI 10.1002/2017GL075583
- 1474 Skeie RB, Berntsen T, Aldrin M, Holden M, Myhre G (2018) Climate sensitivity estimates—
1475 sensitivity to radiative forcing time series and observational data. *Earth Sys Dyn* 9(2):879–
1476 894, DOI 10.5194/esd-9-879-2018
- 1477 Smith DM, Booth BBB, Dunstone NJ, Eade R, Hermanson L, Jones GS, Scaife AA, Sheen KL,
1478 Thompson V (2016) Role of volcanic and anthropogenic aerosols in recent slowdown in
1479 global surface warming. *Nature Climate Change* 6:936–940, DOI 10.1038/NCLIMATE3058
- 1480 Stevens B, Sherwood SC, Bony S, Webb MJ (2016) Prospects for narrowing bounds on earth’s
1481 equilibrium climate sensitivity. *Earth’s Future* 4:512–522, DOI 10.1002/2016EF000376
- 1482 Tett SFB, Betts R, Crowley TJ, Gregory J, Johns TC, Jones A, Osborn TJ, Öström E, Roberts
1483 DL, Woodage MJ (2007) The impact of natural and anthropogenic forcings on climate and
1484 hydrology. *Clim Dyn* 28(1):3–34, DOI 10.1007/s00382-006-0165-1
- 1485 Webb MJ, Andrews T, Bodas-Salcedo A, Bony S, Bretherton CS, Chadwick R, Chepfer H,
1486 Douville H, Good P, Kay JE, Klein SA, Marchand R, Medeiros B, Siebesma AP, Skinner
1487 CB, Stevens B, Tselioudis G, Tsushima Y, Watanabe M (2017) The Cloud Feedback
1488 Model Intercomparison Project (CFMIP) contribution to CMIP6. *Geosci Model Devel*
1489 10():359–384, DOI 10.5194/gmd-10-359-2017
- 1490 Xie SP, Kosaka Y (2017) What caused the global surface warming hiatus of 1998–2013? *Current*
1491 *Climate Change Reports* 3:128–140, DOI 10.1007/s40641-017-0063-0
- 1492 Yuan T, Oreopoulos L, Platnick SE, Meyer K (2018) Observations of local positive low cloud
1493 feedback patterns and their role in internal variability and climate sensitivity. *Geophys*
1494 *Res Lett* 45, DOI 10.1029/2018GL077904
- 1495 Zelinka MD, Andrews T, Forster PM, Taylor KE (2014) Quantifying components of aerosol-
1496 cloud-radiation interactions in climate models. *J Geophys Res* 119(12):7599–7615, DOI
1497 10.1002/2014jd021710

-
- 1498 Zhou C, Zelinka MD, Dessler AE, Klein SA (2015) The relationship between inter-
1499 annual and long-term cloud feedbacks. *Geophys Res Lett* 42:10,46310,469, DOI
1500 10.1002/2015GL066698
- 1501 Zhou C, Zelinka MD, Klein SA (2016) Impact of decadal cloud variations on the Earth's energy
1502 budget. *Nature Geosci* 9:871–875, DOI 10.1038/NGEO2828